Fourier Circuits in Neural Networks and Transformers: A Case Study of Modular Arithmetic with Multiple Inputs

Chenyang Li[1] **Yingyu Liang**[2,3] **Zhenmei Shi**[3] **Zhao Song**[4] **Tianyi Zhou**[5]

[1]Fuzhou University. [2]The University of Hong Kong. [3]University of Wisconsin-Madison.
[4]The Simons Institute for the Theory of Computing at the UC, Berkeley. [5]University of Southern California.

Abstract

In the evolving landscape of machine learning, a pivotal challenge lies in deciphering the internal representations harnessed by neural networks and Transformers. Building on recent progress toward comprehending how networks execute distinct target functions, our study embarks on an exploration of the underlying reasons behind networks adopting specific computational strategies. We direct our focus to the complex algebraic learning task of modular addition involving k inputs. Our research presents a thorough analytical characterization of the features learned by stylized one-hidden layer neural networks and one-layer Transformers in addressing this task. A cornerstone of our theoretical framework is the elucidation of how the principle of margin maximization shapes the features adopted by one-hidden layer neural networks. Let p denote the modulus, D_p denote the dataset of modular arithmetic with k inputs and m denote the network width. We demonstrate that a neuron count of $m \geq 2^{2k-2} \cdot (p-1)$, these networks attain a maximum $L_{2,k+1}$-margin on the dataset D_p. Furthermore, we establish that each hidden-layer neuron aligns with a specific Fourier spectrum, integral to solving modular addition problems. By correlating our findings with the empirical observations of similar studies, we contribute to a deeper comprehension of the intrinsic computational mechanisms of neural networks. Furthermore, we observe similar computational mechanisms in attention matrices of one-layer Transformers. Our work stands as a significant stride in unraveling their operation complexities, particularly in the realm of complex algebraic tasks.

1 INTRODUCTION

The field of artificial intelligence has experienced a significant transformation with the development of large language models (LLMs), particularly through the introduction of the Transformer architecture (Vaswani et al., 2017). This advancement has revolutionized approaches to challenging tasks in natural language processing, notably in machine translation (Prato et al., 2020; Gao et al., 2020) and text generation (Luo et al., 2022). Consequently, models e.g., Mistral (Jiang et al., 2023), Llama (AI, 2024), Gemini (Team et al., 2023), Gemma (Team et al., 2024), Claude3 (Anthropic, 2024), GPT4 (OpenAI, 2023) and so on, have become predominant in NLP.

Central to this study is the question of how these advanced models transcend mere pattern recognition to engage in what appears to be logical reasoning and problem-solving. This inquiry is not purely academic; it probes the core of "understanding" in artificial intelligence. While LLMs, such as Claude3 and GPT4, demonstrate remarkable proficiency in human-like text generation, their capability to comprehend and process mathematical logic is a topic of considerable debate. This line of investigation is crucial, given AI's potential to extend beyond text generation into deeper comprehension of complex subjects. Mathematics, often seen as the universal language, presents a uniquely challenging domain for these models (Yousefzadeh and Cao, 2023). Our research aims to determine whether Transformers with attention, noted for their NLP efficiency, can also demonstrate an intrinsic understanding of mathematical operations and reasoning.

In a recent surprising study of mathematical operations learning, Power et al. (2022) train Transformers on small algorithmic datasets, e.g., $a_1 + a_2 \mod p$ and

Proceedings of the 28th International Conference on Artificial Intelligence and Statistics (AISTATS) 2025, Mai Khao, Thailand. PMLR: Volume 258. Copyright 2025 by the author(s).

we let p be a prime number, and show the "grokking" phenomenon, where models abruptly transition from bad generalization to perfect generalization after a large number of training steps. Nascent studies, such as those by Nanda et al. (2023a), empirically reveal that Transformers can solve modular addition using Fourier-based circuits. They found that the Transformers trained by Stochastic Gradient Descent (SGD) not only reliably compute $a_1+a_2 \mod p$, but also that the networks consistently employ a specific geometric algorithm. This algorithm, which involves composing integer rotations around a circle, indicates an inherent comprehension of modular arithmetic within the network's architecture. The algorithm relies on this identity: for any a_1, a_2 and $\zeta \in \mathbb{Z}_p \backslash \{0\}$, the following two quantities are equivalent

$$(a_1 + a_2) \bmod p = \arg\max_{c \in \mathbb{Z}_p} \{\cos(2\pi\zeta(a_1 + a_2 - c)/p)\}.$$

Nanda et al. (2023a) further show that the attention and MLP module in the Transformer imbues the neurons with Fourier circuit-like properties. To study why networks arrive at Fourier-based circuits computational strategies, Morwani et al. (2024) theoretically study one-hidden layer neural network learning on two inputs modular addition task and certify that the trained networks will execute modular addition by employing Fourier features aligning closely with the previous empirical observations. However, the question remains whether neural networks can solve more complicated mathematical problems.

Inspired by recent developments in mechanistic interpretability (Olah et al., 2020; Elhage et al., 2021, 2022) and the study of inductive biases (Soudry et al., 2018; Vardi, 2023) in neural networks, we extend our research to modular addition with more (k) inputs.

$$(a_1 + a_2 + \cdots + a_k) \bmod p. \tag{1}$$

This approach offers insights into why certain representations and solutions emerge from neural network training. By integrating these insights with our empirical findings, we aim to provide a comprehensive understanding of neural networks' learning mechanisms, especially in solving the modular addition problem. We also determine the necessary number of neurons for the network to learn this Fourier method for modular addition. Our paper's contributions are summarized as follows:

- **Expansion of Input for Modular Addition Problem:** We extend the input parameter range for the modular addition problem from a binary set to k-element sets.
- **Network's Maximum Margin:** For p-modular addition of k inputs, we give the closed form of the maximum margin of a network (Lemma 4.2):

$$\gamma^* = \frac{2(k!)}{(2k+2)^{(k+1)/2}(p-1)p^{(k-1)/2}}.$$

- **Neuron Count in One-Hidden-Layer Networks:** We propose that in a general case, a one-hidden-layer network having $m \geq 2^{2k-2} \cdot (p-1)$ neurons can achieve the maximum $L_{2,k+1}$-margin solution, each hidden neuron aligning with a specific Fourier spectrum. This ensures the network's capability to effectively solve the modular addition in a Fourier-based method (Theorem 4.1).
- **Empirical Validation of Theoretical Findings:** We validate our theoretical finding that: when $m \geq 2^{2k-2} \cdot (p-1)$, for each spectrum $\zeta \in \{1, \ldots, \frac{p-1}{2}\}$, there exists a hidden-neuron utilizes this spectrum. It strongly supports our analysis. (Figure 1 and Figure 2).
- **Similar Findings in Transformer:** We have a similar observation in one-layer Transformer learning modular addition involving k inputs. For the 2-dimensional matrix $W_K W_Q$, where W_K, W_Q denotes the key and query matrix, it shows the superposition of two cosine waveforms in each dimension, each characterized by distinct frequencies (Figure 3).
- **Grokking under Different k:** We observe that as k increases, the grokking phenomenon becomes weaker, as predicted by our analysis (Figure 4).

Detailed comparison with Morwani et al. (2024). Theoretically, we generalize beyond the results of Morwani et al. (2024) to k inputs. There are unique technique challenges for our setting and not presented in previous settings: (1) While constructing a general k version of the max-margin solution, we need our unique sum-to-product Identities for k inputs, which was proved by our Lemma E.1; (2) To calculate the number of neurons, we need our unique Lemma 4.3 and Eq (25) to handle cosine operation on k inputs; (3) We need our Lemma D.7 and Lemma D.8 to handle multiple variable Fourier transform, where we also introduce multiple inequalities for k inputs version. Empirically, our experiments verified that the theoretical insight obtained can be carried over to practical transformers. Furthermore, the study of grokking is beyond Morwani et al. (2024), as the study of grokking is only possible when there are $k \geq 2$. Our general k version is necessary for studying some key properties of network learning, like grokking over tasks of increasing complexity or generalization ability over tasks of increasing complexity.

2 RELATED WORK

Max Margin Solutions in Neural Networks. Bronstein et al. (2022) demonstrated that neurons in a one-hidden-layer ReLU network align with clauses in max margin solutions for read-once DNFs, employing a unique proof technique involving the construction of perturbed networks. Morwani et al. (2024) utilize max-min duality to certify maximum-margin solutions. Further, extensive research in the domain of margin maximization in neural networks, including works by Gunasekar et al. (2018b); Soudry et al. (2018); Gunasekar et al. (2018a); Wei et al. (2019b); Lyu and Li (2019); Ji and Telgarsky (2019); Moroshko et al. (2020); Chizat and Bach (2020); Ji and Telgarsky (2020); Lyu et al. (2021); Frei et al. (2022b, 2023); Shi et al. (2023b); Li et al. (2024a) and more, has highlighted the implicit bias towards margin maximization inherent in neural network optimization. They provide a foundational understanding of the dynamics of neural networks and their inclination towards maximizing margins under various conditions and architectures.

Algebraic Tasks Learning Mechanism Interpretability. The study of neural networks trained on algebraic tasks has been pivotal in shedding light on their training dynamics and inductive biases. Notable contributions include the work of Power et al. (2022); Gromov (2023); Quirke and Barez (2023) on modular addition and subsequent follow-up studies, investigations into learning parities (Daniely and Malach, 2020; Barak et al., 2022; Shi et al., 2022, 2024b, 2023c,a; Zhang et al., 2023; Xu et al., 2024b), and research into algorithmic reasoning capabilities (Saxton et al., 2018; Hendrycks et al., 2021; Lewkowycz et al., 2022; Meng et al., 2022; Damian et al., 2022; Chughtai et al., 2023; Stander et al., 2023; Nanda et al., 2023b; Zhong et al., 2023; Tigges et al., 2023; Hanna et al., 2023). The field of mechanistic interpretability, focusing on the analysis of internal representations in neural networks, has also seen significant advancements through the works of Cammarata et al. (2020); Olsson et al. (2022); Merrill et al. (2023); Rubin et al. (2023); Varma et al. (2023); Doshi et al. (2024); Shi et al. (2024a); Ke et al. (2024); Chen et al. (2024); Liang et al. (2024b); Saxena et al. (2024); Ke et al. (2025); Chen et al. (2025); Liang et al. (2025); Li et al. (2025) and others.

Grokking and Emergent Ability. The phenomenon known as "grokking" was initially identified by Power et al. (2022) and is believed to be a way of studying the emerging abilities of LLM (Wei et al., 2022). This research observed a unique trend in two-layer transformer models engaged in algorithmic tasks, where there was a significant increase in test accuracy, surprisingly occurring well after these models had reached perfect accuracy in their training phase. In Millidge (2022), it was hypothesized that this might be the result of the SGD process that resembles a random path along what is termed the optimal manifold. Adding to this, Nanda et al. (2023a) aligns with the findings of Belinkov (2022), indicating a steady advancement of networks towards algorithms that are better at generalization. Liu et al. (2022); Xu et al. (2024a); Lyu et al. (2024) developed smaller-scale examples of grokking and utilized these to map out phase diagrams, delineating multiple distinct learning stages. Furthermore, Thilak et al. (2022); Murty et al. (2023) suggested the possibility of grokking occurring naturally, even in the absence of explicit regularization. They attributed this to an optimization quirk they termed the slingshot mechanism, which might inadvertently act as a regularizing factor.

Theoretical Work About Fourier Transform. To calculate Fourier transform there are two main methodologies: one uses carefully chosen samples through hashing functions (referenced in works like Indyk et al. (2014); Indyk and Kapralov (2014); Kapralov (2016, 2017)) to achieve sublinear sample complexity and running time, while the other uses random samples (as discussed in Bourgain (2014); Haviv and Regev (2017); Nakos et al. (2019)) with sublinear sample complexity but nearly linear running time. There are many other works studying Fourier transform (Song, 2019; Jin et al., 2023; Gao et al., 2022; Lee et al., 2019; Chen et al., 2020; Song et al., 2022; Chen et al., 2016; Song et al., 2023a; Chen et al., 2023; Song et al., 2023b; Liang et al., 2024a).

3 PROBLEM SETUP

3.1 Data and Network Setup

Data. Following Morwani et al. (2024), let $\mathbb{Z}_p = [p]$ denote the modular group on p integers, where $p > 2$ is a given prime number. The input space is $\mathcal{X} := \mathbb{Z}_p^k$ for some integer k, and the output space is $\mathcal{Y} := \mathbb{Z}_p$. Then an input data point is $a = (a_1, \dots, a_k)$ with $a_i \in \mathbb{Z}_p$. When clear from context, we also let $x_i \in \{0,1\}^p$ be the one-hot encoding of a_i, and let $x = (x_1, \dots, x_k)$ denote the input point.

Network. We consider single-hidden layer neural networks with polynomial activation functions:

$$f(\theta, x) := \sum_{i=1}^{m} \phi(\theta_i, x), \tag{2}$$

$$\phi(\theta_i, x) := (u_{i,1}^\top x_1 + \cdots + u_{i,k}^\top x_k)^k w_i,$$

where $\theta := \{\theta_1, \dots, \theta_m\} \in \mathbb{R}^{(k+1)\times p}$, $\phi(\theta_i, x)$ is one neuron, and $\theta_i := \{u_{i,1}, \dots, u_{i,k}, w_i\}$ are the parameters of the neuron with $u_{i,1}, \dots, u_{i,k}, w_i \in \mathbb{R}^p$. We use polynomial activation functions due to the homogeneous requirement in Lemma 3.7 and easy sum-to-product identities calculation in Fourier analysis. Using the notation a instead of the one-hot encodings x, we can also write:

$$f(\theta, a) := \sum_{i=1}^{m} \phi(\theta_i, a),$$
$$\phi(\theta_i, a) := (u_{i,1}(a_1) + \cdots + u_{i,k}(a_k))^k w_i,$$

where with $u_{i,j}(a_j)$ being the a_j-th component of $u_{i,j}$. We consider the parameter set:

$$\Theta := \{\|\theta\|_{2,k+1} \leq 1\},$$
$$\text{where } \|\theta\|_{2,k+1} := (\sum_{i=1}^{m} \|\theta_i\|_2^{k+1})^{\frac{1}{k+1}},$$
$$\|\theta_i\|_2 := (\sum_{j=1}^{k} \|u_{i,j}\|_2^2 + \|w_i\|_2^2)^{\frac{1}{2}}.$$

Here $\|\theta\|_{2,k+1}$ is the $L_{2,k+1}$ matrix norm of θ (Definition B.2), and $\|\theta_i\|_2$ is the L_2 vector norm of the concatenated vector of the parameters in θ_i. The training objective over Θ is then as follows.

Definition 3.1. *Given a dataset D_p and the cross-entropy loss l, the regularized training objective is:*

$$\mathcal{L}_\lambda(\theta) := \frac{1}{|D_p|} \sum_{(x,y)\in D_p} l(f(\theta, x), y) + \lambda \|\theta\|_{2,k+1}.$$

3.2 Margins of the Neural Networks

Now, we define the margin for a data point and the margin for a whole dataset.

Definition 3.2. *We denote $g : \mathbb{R}^U \times \mathcal{X} \times \mathcal{Y} \to \mathbb{R}$ as the margin function, where for given $(x, y) \in D_p$,*

$$g(\theta, x, y) := f(\theta, x)[y] - \max_{y' \in \mathcal{Y}\setminus\{y\}} f(\theta, x)[y'].$$

Definition 3.3. *The margin for a given dataset D_p is denoted as $h : \mathbb{R}^U \to \mathbb{R}$ where*

$$h(\theta) := \min_{(x,y)\in D_p} g(\theta, x, y).$$

For parameter θ, its normalized margin is denoted as $h(\theta/\|\theta\|_{2,k+1})$. For simplicity, we define γ^* to be the maximum normalized margin as the following:

Definition 3.4. *The minimum of the regularized objective is denoted as $\theta_\lambda \in \arg\min_{\theta\in\mathbb{R}^U} \mathcal{L}_\lambda(\theta)$. We define the normalized margin of θ_λ as $\gamma_\lambda := h(\theta_\lambda/\|\theta_\lambda\|_{2,k+1})$ and the maximum normalized margin as $\gamma^* := \max_{\theta\in\Theta} h(\theta)$, where $\Theta = \{\|\theta\|_{2,k+1} \leq 1\}$.*

Let $\mathcal{P}(D_p)$ denote a set containing all distributions over D_p. Then γ^* can be rewritten as

$$\begin{aligned}\gamma^* &= \max_{\theta\in\Theta} h(\theta) = \max_{\theta\in\Theta} \min_{(x,y)\in D_p} g(\theta, x, y) \\ &= \max_{\theta\in\Theta} \min_{q\in\mathcal{P}(D_p)} \mathop{\mathbb{E}}_{(x,y)\sim q} [g(\theta, x, y)], \end{aligned} \tag{3}$$

where the first step is from Definition 3.4, the second step is from Definition 3.3, and the last step is from the linearity of the expectation. Now, we introduce an important concept of a duality stationary pair (θ^*, q^*).

Definition 3.5. *We define a stationary pair (θ^*, q^*) when satisfying*

$$\begin{aligned} q^* &\in \arg\min_{q\in\mathcal{P}(D_p)} \mathop{\mathbb{E}}_{(x,y)\sim q} [g(\theta^*, x, y)], \\ \theta^* &\in \arg\min_{\theta\in\Theta} \mathop{\mathbb{E}}_{(x,y)\sim q^*} [g(\theta, x, y)]. \end{aligned} \tag{4}$$

This means that q^* is a distribution that minimizes the expected margin based on θ^*, and simultaneously, θ^* is a solution that maximizes the expected margin relative to q^*. The max-min inequality (Boyd and Vandenberghe, 2004) indicates that presenting such a duality adequately proves θ^* to be a maximum margin solution. Recall that there is a "max" operation in Definition 3.2, which makes the swapping of expectation and summation infeasible, meaning that the expected network margin cannot be broken down into the expected margins of individual neurons. To tackle this problem, the class-weighted margin is proposed, whose intuition is similar to label smoothing. Let $\tau : D_p \to \Delta(\mathcal{Y})$ allocate weights to incorrect labels for every data point. Given (x, y) in D_p and for any $y' \in \mathcal{Y}$, we have $\tau(x, y)[y'] \geq 0$ and $\sum_{y'\in\mathcal{Y}\setminus\{y\}} \tau(x, y)[y'] = 1$. We denote a proxy g' as the following to solve the issue.

Definition 3.6. *Draw $(x, y) \in D_p$. The class-weighted margin g' is defined as*

$$g'(\theta, x, y) := f(\theta, x)[y] - \sum_{y'\in\mathcal{Y}\setminus\{y\}} \tau(x, y)[y'] f(\theta, x)[y'].$$

We have g' uses a weighted sum rather than max, so $g(\theta, x, y) \leq g'(\theta, x, y)$. Following the linearity of expectation, we get the expected class-weighted margin as

$$\begin{aligned}\mathop{\mathbb{E}}_{(x,y)} [g'(\theta, x, y)] = \sum_{i=1}^{m} \mathop{\mathbb{E}}_{(x,y)} \Big[&\phi(\theta_i, x)[y] \\ &- \sum_{y'\in\mathcal{Y}\setminus\{y\}} \tau(x, y)[y'] \phi(\theta_i, x)[y']\Big],\end{aligned}$$

where we can move the summation $\sum_{i=1}^{m}$ out of the expectation $\mathbb{E}[]$.

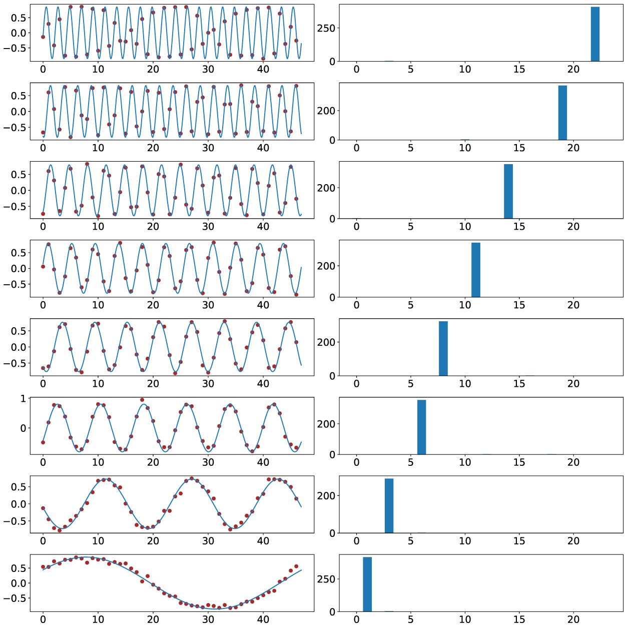

Figure 1: Cosine shape of the trained embeddings (hidden layer weights) and corresponding power of Fourier spectrum. The two-layer network with $m = 2944$ neurons is trained on k = 4-sum mod-p = 47 addition dataset. We even split the whole datasets ($p^k = 47^4$ data points) into the training and test datasets. Every row represents a random neuron from the network. The left figure shows the final trained embeddings, with red dots indicating the true weight values, and the pale blue interpolation is achieved by identifying the function that shares the same Fourier spectrum. The right figure shows their Fourier power spectrum. The results in these figures are consistent with our analysis statements in Lemma 4.2. See Figure 5, 7 in Appendix H.2 for similar results when k is 3 or 5.

3.3 Connection between Training and the Maximum Margin Solutions

We denote ν as the network's homogeneity constant, where the equation $f(\alpha\theta, x) = \alpha^\nu f(\theta, x)$ holds for any x and any scalar $\alpha > 0$. Specifically, we focus on networks with homogeneous neurons that satisfy $\phi(\alpha\theta_i, x) = \alpha^\nu \phi(\theta_i, x)$ for any $\alpha > 0$. Note that our one-hidden layer networks (Eq. (2)) are $k + 1$ homogeneous. As the following Lemma states, when λ is small enough during training homogeneous functions, we have the $\mathcal{L}_\lambda$ global optimizers' normalized margin converges to γ^*.

Lemma 3.7 (Wei et al. (2019a), Theorem 4.1)**.** *Let f be a homogeneous function. For any norm $\|\cdot\|$, if $\gamma^* > 0$, we have $\lim_{\lambda\to 0} \gamma_\lambda = \gamma^*$.*

Therefore, to comprehend the global minimize, we can explore the maximum-margin solution as a surrogate, enabling us to bypass complex analyses in nonconvex optimization. Furthermore, Morwani et al. (2024) states that under the following condition, the maximum-margin solutions and class-weighted maximum-margin (g') solutions are equivalent to each other.

Condition 3.8 (Condition C.1 in page 8 in Morwani et al. (2024))**.** *We have $g'(\theta^*, x, y) = g(\theta^*, x, y)$ for all $(x, y) \in \operatorname{spt}(q^*)$, where* spt *is the support. It means:*

$$\{y' \in \mathcal{Y}\backslash\{y\} : \tau(x, y)[y'] > 0\} \subseteq \underset{y'\in\mathcal{Y}\backslash\{y\}}{\arg\max} f(\theta^*, x)[y'].$$

Thus, under these conditions, we only need to focus on the class-weighted maximum-margin solutions in our following analysis.

4 MAIN RESULT

We characterize the Fourier features to perform modular addition with k input in the one-hidden-layer neuron network. We show that every neuron only focuses on a distinct Fourier frequency. Additionally, within the network, there is at least one neuron for each frequency. When we consider the uniform class weighting, where $\mathcal{L}_\lambda(\theta)$ is based on

$$\tau(a_1, \ldots, a_k)[c'] := 1/(p-1) \quad \forall c' \neq a_1 + \cdots + a_k, \tag{5}$$

we have the following main result:

Theorem 4.1 (Main result, informal version of Theorem G.2)**.** *Let $f(\theta, x)$ be the one-hidden layer networks defined in Eq* (2)*. If $m \geq 2^{2k-1} \cdot \frac{p-1}{2}$, then the max $L_{2,k+1}$-margin network satisfies:*

- *The maximum $L_{2,k+1}$-margin for a dataset D_p is:*

$$\gamma^* = \frac{2(k!)}{(2k+2)^{(k+1)/2}(p-1)p^{(k-1)/2}}.$$

- *For each neuron $\phi(\{u_1, \ldots, u_k, w\}; a_1, \ldots, a_k)$, there is a constant scalar $\beta \in \mathbb{R}$ and a frequency $\zeta \in \{1, \ldots, \frac{p-1}{2}\}$ satisfying*

$$u_i(a_i) = \beta \cdot \cos(\theta^*_{u_i} + 2\pi\zeta a_i/p), \quad \forall i \in [k]$$
$$w(c) = \beta \cdot \cos(\theta^*_w + 2\pi\zeta c/p),$$

  where $\theta^*_{u_1}, \ldots, \theta^*_{u_k}, \theta^*_w \in \mathbb{R}$ are some phase offsets satisfying $\theta^*_{u_1} + \cdots + \theta^*_{u_k} = \theta^*_w$.

- *For each frequency $\zeta \in \{1, \ldots, \frac{p-1}{2}\}$, there exists one neuron using this frequency only.*

Proof sketch of Theorem 4.1. See formal proof in Appendix G.2. By Lemma 4.2, we get γ^* and the single-neuron class-weighted maximum-margin solution set

$\Omega_q^{'*}$. By satisfying Condition 3.8, we know it is used in the maximum-margin solution. By Lemma 4.3, we can construct the network θ^* that uses neurons in $\Omega_q^{'*}$. By Lemma C.2, we know that it is the maximum-margin solution. Finally, by Lemma F.2, we know that all frequencies are covered. □

Theorem 4.1 tells us when the number of neurons is large enough, e.g., $m \geq 2^{2k-1} \cdot \frac{p-1}{2}$ (the lower bound of m may not be the tightest in our analysis), the one hidden neural network will exactly learn all Fourier spectrum/basis to recover the modular addition operation. More specifically, each neuron will only focus on one Fourier frequency. Our analysis provides a comprehensive understanding of why neural networks trained by SGD prefer to learn Fourier-based circuits.

Our analysis essentially provides hints on how neural networks learn to perform well. Note that humans do modular calculations completely differently with Fourier circuits. Thus, for more general tasks, the model behavior may differ from that of human beings. On the other hand, the Fourier spectrum feature pattern could be useful for out-of-distribution (OOD), robust learning, or designing better learning algorithms, e.g., making the implicit regularization explicit.

4.1 Technique Overview

In this section, we propose techniques overview of the proof for our main result. We use $\mathbf{i}$ to denote $\sqrt{-1}$. Let $f : \mathbb{Z}_p \to \mathbb{C}$. Then, for each frequency $j \in \mathbb{Z}_p$, we define f discrete Fourier transform (DFT) as $\widehat{f}(j) := \sum_{\zeta\in\mathbb{Z}_p} f(\zeta) \exp(-2\pi\mathbf{i} \cdot j\zeta/p)$. Let $\Omega_q^{'*}$ be the single neuron class-weighted maximum-margin solution set (formally defined in Definition D.6).

First, we provide a brief informal high-level intuition of our proof. Based on Condition 3.8 (proved by Lemma 4.3), the maximum-margin solutions and class-weighted maximum-margin are equivalent to each other. Thus, in Lemma 4.2, we can get the class-weighted maximum-margin solution as the problem has been reduced from a network max-margin problem to a single-neuron max-margin problem. Finally, combining all of these, we have our main Theorem 4.1.

Now, we show how to get $\Omega_q'^*$.

Lemma 4.2 (Informal version of Lemma D.8)**.** *If for any $\zeta \in \{1, \dots, \frac{p-1}{2}\}$, there exists a scaling constant $\beta \in \mathbb{R}$, such that $u_i(a_i) = \beta \cdot \cos(\theta^*_{u_i} + 2\pi\zeta a_i/p)$ for any $i \in [k]$ and $w(c) = \beta \cdot \cos(\theta^*_w + 2\pi\zeta c/p)$, where $\theta^*_{u_1}, \dots, \theta^*_{u_k}, \theta^*_w \in \mathbb{R}$ are some phase offsets satisfying $\theta^*_{u_1} + \dots + \theta^*_{u_k} = \theta^*_w$. Then, we have $\Omega_q'^* = \{(u_1, \dots, u_k, w)\}$, and $\gamma^* = \frac{2(k!)}{(2k+2)^{(k+1)/2}(p-1)p^{(k-1)/2}}$.*

Proof sketch of Lemma 4.2. See formal proof in Appendix D.5. The proof establishes the maximum-margin solution's sparsity in the Fourier domain through several key steps. Initially, by Lemma D.7, focus is directed to maximizing Eq. (15). For odd p, Eq. (15) can be reformulated with magnitudes and phases of $\widehat{u}_i$ and $\widehat{w}$ (discrete Fourier transform of u_i and w), leading to an equation involving cosine of their phase differences. Plancherel's theorem is then employed to translate the norm constraint to the Fourier domain. This allows for the optimization of the cosine term in the sum, effectively reducing the problem to maximizing the product of magnitudes of $\widehat{u}_i$ and $\widehat{w}$ (Eq. (19)). By applying the inequality of arithmetic and geometric means, we have an upper bound for the optimization problem. To achieve the upper bound, equal magnitudes are required for all $\widehat{u}_i$ and $\widehat{w}$ at a single frequency, leading to Eq. (21). The neurons are finally expressed in the time domain, demonstrating that they assume a specific cosine form with phase offsets satisfying certain conditions. □

Next, we show the number of neurons required to solve the problem and the properties of these neurons. We demonstrate how to use these neurons to construct the network θ^*.

Lemma 4.3 (Informal version of Lemma E.3)**.** *Let $\cos_\zeta(x)$ denote $\cos(2\pi\zeta x/p)$. Then, we have the maximum $L_{2,k+1}$-margin solution θ^* will consist of $2^{2k-1} \cdot \frac{p-1}{2}$ neurons $\theta^*_i \in \Omega_q^{'*}$ to simulate $\frac{p-1}{2}$ type of cosine computation, where each cosine computation is uniquely determined a $\zeta \in \{1, \dots, \frac{p-1}{2}\}$. In particular, for each ζ the cosine computation is $\cos_\zeta(a_1 + \dots + a_k - c), \forall a_1, \dots, a_k, c \in \mathbb{Z}_p$.*

Proof sketch of Lemma 4.3. See formal proof in Appendix E.3. Our goal is to show that $2^{2k-1} \cdot \frac{p-1}{2}$ neurons $\theta^*_i \in \Omega_q^{'*}$ are able to simulate $\frac{p-1}{2}$ type of cos computation. We have the following expansion function of $\cos_\zeta(x)$, which denotes $\cos(2\pi\zeta x/p)$.

$$\cos_\zeta(\sum_{i=1}^k a_i) = \sum_{b\in\{0,1\}^k} \prod_{i=1}^k \cos^{1-b_i}(a_i) \cdot \sin^{b_i}(a_i) \cdot \mathbf{1}[\sum_{i=1}^k b_i\%2 = 0] \cdot (-1)^{\mathbf{1}[\sum_{i=1}^k b_i\%4=2]}.$$

The above equation can decompose a $\cos(\sum)$ to some basic elements. We have 2^k terms in the above equation. By using the following fact in Lemma E.1,

$$2^k \cdot k! \cdot \prod_{i=1}^k a_i = \sum_{c\in\{-1,+1\}^k} (-1)^{(k-\sum_{i=1}^k c_i)/2} (\sum_{j=1}^k c_j a_j)^k,$$

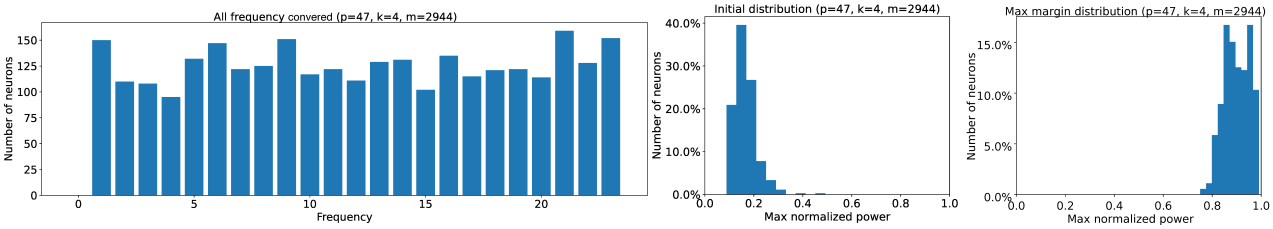

(a) (b) (c)

Figure 2: All Fourier spectrum frequencies being covered and the maximum normalized power of the embeddings (hidden layer weights). The one-hidden layer network with $m = 2944$ neurons is trained on $k = 4$-sum mod-$p = 47$ addition dataset. We denote $\widehat{u}[i]$ as the Fourier transform of $u[i]$. Let $\max_i |\widehat{u}[i]|^2/(\sum |\widehat{u}[j]|^2)$ be the maximum normalized power. Mapping each neuron to its maximum normalized power frequency, (a) shows the final frequency distribution of the embeddings. Similar to our construction analysis in Lemma 4.3, we have an almost uniform distribution over all frequencies. (b) shows the maximum normalized power of the neural network with random initialization. (c) shows, in frequency space, the embeddings of the final trained network are one-sparse, i.e., maximum normalized power being almost 1 for all neurons. This is consistent with our max-margin analysis results in Lemma 4.3. See Figure 6 and 8 in Appendix H.2 for results when k is 3 or 5.

where each term can be constructed by 2^{k-1} neurons. Therefore, we need $2^{k-1}2^k$ total neurons. To simulate $\frac{p-1}{2}$ type of simulation, we need $2^{2k-1}\frac{p-1}{2}$ neurons. Then, using the Lemma C.1, we construct the network θ^*. By using the Lemma C.2 from Morwani et al. (2024), we get it is the maximum-margin solution. □

5 EXPERIMENTS

First, we conduct simulation experiments to verify our analysis for $k = 3, 4, 5$. Then, we show that the one-layer transformer learns 2-dimensional cosine functions in their attention weights. Finally, we show the grokking phenomenon under different k. Please refer to Appendix H.1 for details about implementation.

5.1 One-hidden Layer Neural Network

We conduct simulation experiments to verify our analysis. In Figure 1 and Figure 2, we use SGD to train a two-layer network with $m = 2944 = 2^{2k-2} \cdot (p-1)$ neurons, i.e., Eq. (2), on $k = 4$-sum mod-$p = 47$ addition dataset, i.e., Eq. (1). Figure 1 shows that the networks trained with SGD have single-frequency hidden neurons, which support our analysis in Lemma 4.2. Furthermore, Figure 2 demonstrates that the network will learn all frequencies in the Fourier spectrum, which is consistent with our analysis in Lemma 4.3. Together, they verify our main results in Theorem 4.1 and show that the network trained by SGD prefers to learn Fourier-based circuits. There are more similar results when k is 3 or 5 in Appendix H.2.

5.2 One-layer Transformer

We find similar results in one-layer transformers. Let E be input embedding and W^P, W^V, W^K, W^Q be projection, value, key and query matrix. The m-heads attention layer can be written as

$$W^P \begin{pmatrix} W_1^{V\top} E \cdot \mathrm{softmax}\left(E^\top W_1^K W_1^{Q\top} E\right) \\ \cdots \\ W_m^{V\top} E \cdot \mathrm{softmax}\left(E^\top W_m^K W_m^{Q\top} E\right) \end{pmatrix}.$$

We denote $W^K W^{Q\top}$ as W^{KQ} and call it attention matrix. In Figure 3, we train a one-layer transformer with $m = 160$ heads attention and hidden dimension 128, i.e., above equation, on $k = 4$-sum mod-$p = 31$ addition dataset, i.e., Eq. (1). Figure 3 shows that the SGD-trained one-layer transformer learns 2-dim cosine shape attention matrices, which is similar to the one-hidden layer neural networks in Figure 1. This means that the attention layer has a learning mechanism similar to neural networks in the modular arithmetic task. It prefers to learn (2-dim) Fourier-based circuits when trained by SGD. There are more similar results when k is 3 or 5 in Appendix H.3.

5.3 Grokking under Different k

To support the importance of our data setting, we study the grokking phenomenon in our data distribution. Following the experiments' protocol in Power et al. (2022), we show there is the grokking phenomenon under different k. We train two-layer transformers with $m = 160$ attention heads and hidden dimension as 128 on $k = 2, 3, 4, 5$-sum mod-$p = 97, 31, 11, 5$ addition dataset with 50% of the data in training. We use different p to guarantee the dataset

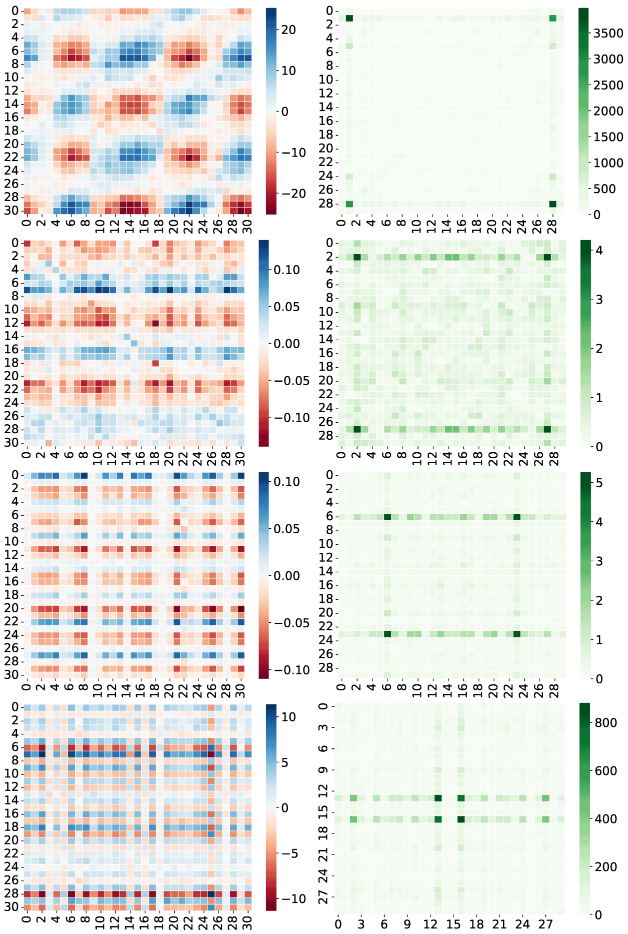

Figure 3: 2-dimension cosine shape of the trained W^{KQ} (attention weights) and their Fourier power spectrum. The one-layer transformer with attention heads $m = 160$ is trained on $k = 4$-sum mod-$p = 31$ addition dataset. We even split the whole datasets ($p^k = 31^4$ data points) into training and test datasets. Every row represents a random attention head from the transformer. The left figure shows the final trained attention weights being an apparent 2-dim cosine shape. The right figure shows their 2-dim Fourier power spectrum. The results in the figures are consistent with Figure 1. See Figure 9 and Figure 10 in Appendix H.3 for similar results when k is 3 or 5.

sizes are roughly equal to each other. Figure 4 shows that the grokking weakens as the number of k increases, which is consistent with our analysis. When k increases, the function class will become more complicated, as we may need more neurons to achieve the max-margin solution. Thus, we use our Theorem 4.1 as a metric to measure the data complexity. It implies that when the ground-truth function class becomes "complicated", the transformers need to train more steps to fit the training datasets, and the generalization tends to be better. Brilliant recent works by Lyu et al. (2024); Kumar et al. (2023) argue that, during learning, the network will be first in the lazy training/NTK regime and then transfer to the rich/feature learning regime sharply, leading to a grokking phenomenon. We use learning steps required for regime switch as a metric of grokking strength.

"Underfitting" in NTK but "overfitting" in Feature Learning. NTK is a notorious overparameterized regime, which probably needs a much larger number of neurons than our max-margin convergence case, i.e., much larger than $\Omega(2^{2k})$ in Theorem 4.1. Thus, under the fixed m and increasing k, the model may easily escape the NTK regime, or there is no longer an NTK regime. Thus, we will see a weaker grokking phenomenon as the learning steps needed to transfer from the NTK regime to the feature learning regime become fewer. With increasing k, the model will have an "underfitting" issue in the NTK regime, meaning the model must need feature learning to fit the task but cannot only fit the task by NTK. However, the model still has an "overfitting" in the feature learning regime.

6 DISCUSSION

6.1 Grokking in Transformers

The interpretability of grokking in Transformers is explored in Nanda et al. (2023a). By examining various intermediate states within the residual stream of the Transformer model, it is validated that the model employs Fourier features to tackle the modular addition task. However, fully comprehending how the Transformer model and LLMs perform modular addition remains challenging based on the current work, particularly from a theoretical standpoint. We contend that beginning with a simplistic model setup and achieving a thorough and theoretical understanding of how the network utilizes Fourier features to address the problem serves as a valuable starting point and it provides a theoretical understanding of the grokking phenomenon. We believe that further study on Transformers will be an interesting and important future direction.

6.2 Grokking, Benign Overfitting, and Implicit Bias

Recently, Xu et al. (2024a) connects the grokking phenomenon to benign overfitting (Bartlett et al., 2020; Cao et al., 2022; Tsigler and Bartlett, 2023; Frei et al., 2022a, 2023). It shows how the network undergoes a grokking period from catastrophic to benign overfitting. Lyu et al. (2024); Kumar et al. (2023) uses implicit bias (Soudry et al., 2018; Gunasekar et al.,

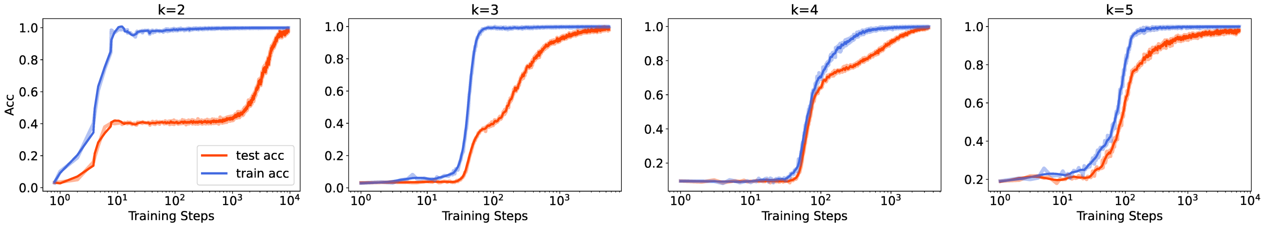

Figure 4: Grokking (models abruptly transition from bad generalization to perfect generalization after a large number of training steps) under learning modular addition involving $k = 2, 3, 4, 5$ inputs. We train two-layer transformers with $m = 160$ attention heads on $k = 2, 3, 4, 5$-sum mod-$p = 97, 31, 11, 5$ addition dataset with 50% of the data in the training set under AdamW Loshchilov and Hutter (2018) optimizer 1e-3 learning rate and 1e-3 weight decay. We use different p to guarantee the dataset sizes are roughly equal to each other. The blue curves show training accuracy, and the red ones show validation accuracy. There is a grokking phenomenon in all figures. However, as k increases, the grokking phenomenon becomes weak. See explanation in Section 5.

2018a; Ji and Telgarsky, 2019; Shah et al., 2020; Moroshko et al., 2020; Chizat and Bach, 2020; Lyu et al., 2021; Jacot, 2022; Xu et al., 2023, 2024c) to explain grokking, where grokking happens if the early phase bias implies an overfitting solution while late phase bias implies a generalizable solution. The intuition from the benign overfitting and the implicit bias well align with our observation in Section 5. It is interesting and valuable to rigorously analyze the grokking or emergent ability under different function class complexities, e.g., Eq (1). We leave this challenge problem as a future work.

6.3 High Order Correlation Attention

Sanford et al. (2023); Alman and Song (2023, 2024); Liang et al. (2024c); Li et al. (2024b); Zhang et al. (2025) state that, when $k = 3$, $a_1 + a_2 + a_3 \bmod p$ is hard to be captured by traditional attention. Thus, they introduce high-order attention to capture high-order correlation from the input sequence. However, in Section 5, we show that one-layer transformers have a strong learning ability and can successfully learn modular arithmetic tasks even when $k = 5$. This implies that the traditional attention may be more powerful than we expect.

6.4 Connection to Parity and SQ Hardness

If we let $p = 2$, then $(a_1 + \cdots + a_k) \bmod p$ will degenerate to parity function, i.e., $b_1, \ldots, b_k \in \{\pm 1\}$ and determining $\prod_{i=1}^k b_i$. Parity functions serve as a fundamental set of learning challenges in computational learning theory, often used to demonstrate computational obstacles (Shalev-Shwartz et al., 2017). In particular, (n, k)-sparse parity problem is notorious hard to learn, i.e., Statistical Query (SQ) hardness (Blum et al., 1994). Daniely and Malach (2020) showed that one-hidden layer networks need an $\Omega(\exp(k))$ number of neurons or an $\Omega(\exp(k))$ number of training steps to successfully learn it by SGD. In our work, we are studying Eq. (2), which is a more general function than parity and indeed is a learning hardness. Our Theorem 4.1 states that we need $\Omega(\exp(k))$ number of neurons to represent the maximum-margin solution, which well aligns with existing works. Our experiential results in Section 5 are also consistent. Hence, our modular addition involving k inputs function class is a good data model to analyze and test the model learning ability, i.e., approximation, optimization, and generalization.

7 CONCLUSION

We study neural networks and transformers learning on $(a_1 + \cdots + a_k) \bmod p$. We theoretically show that networks prefer to learn Fourier circuits. Our experiments on neural networks and transformers support our analysis. Finally, we study the grokking phenomenon under this new data setting.

8 LIMITATIONS

Our work has made progress in exploring how neural networks and Transformers can solve complex mathematical problems such as modular addition operation, but the practical application scope of their conclusions is limited. On the other hand, we admit that our theorem can provide intuition but cannot fully explain the phenomena shown in Figure 4. Thus, we would like to introduce this more general data setting to the community so that we can study and understand grokking in a more broad way. Studying the relationship between the number of neurons and the grokking strength is interesting and important, and we will leave it as our future work.

Acknowledgement

Research is partially supported by the National Science Foundation (NSF) Grants 2008559-IIS, 2023239-DMS, CCF-2046710, and Air Force Grant FA9550-18-1-0166.

References

Meta AI. Introducing meta llama 3: The most capable openly available llm to date, 2024. `https://ai.meta.com/blog/meta-llama-3/`.

Josh Alman and Zhao Song. Fast attention requires bounded entries. In *NeurIPS*. arXiv preprint arXiv:2302.13214, 2023.

Josh Alman and Zhao Song. How to capture higher-order correlations? generalizing matrix softmax attention to kronecker computation. In *The Twelfth International Conference on Learning Representations*, 2024.

Anthropic. The claude 3 model family: Opus, sonnet, haiku, 2024. `https://www-cdn.anthropic.com/de8ba9b01c9ab7cbabf5c33b80b7bbc618857627/Model_Card_Claude_3.pdf`.

Boaz Barak, Benjamin Edelman, Surbhi Goel, Sham Kakade, Eran Malach, and Cyril Zhang. Hidden progress in deep learning: Sgd learns parities near the computational limit. *Advances in Neural Information Processing Systems*, 35:21750–21764, 2022.

Peter L Bartlett, Philip M Long, Gábor Lugosi, and Alexander Tsigler. Benign overfitting in linear regression. *Proceedings of the National Academy of Sciences*, 117(48):30063–30070, 2020.

Yonatan Belinkov. Probing classifiers: Promises, shortcomings, and advances. *Computational Linguistics*, 48(1):207–219, March 2022. doi: 10.1162/coli_a_00422.

Avrim Blum, Merrick Furst, Jeffrey Jackson, Michael Kearns, Yishay Mansour, and Steven Rudich. Weakly learning dnf and characterizing statistical query learning using fourier analysis. In *Proceedings of the twenty-sixth annual ACM symposium on Theory of computing*, pages 253–262, 1994.

Jean Bourgain. An improved estimate in the restricted isometry problem. In *Geometric aspects of functional analysis*, pages 65–70. Springer, 2014.

Stephen P Boyd and Lieven Vandenberghe. *Convex optimization*. Cambridge university press, 2004.

Ido Bronstein, Alon Brutzkus, and Amir Globerson. On the inductive bias of neural networks for learning read-once dnfs. In *Uncertainty in Artificial Intelligence*, pages 255–265. PMLR, 2022.

Nick Cammarata, Gabriel Goh, Shan Carter, Ludwig Schubert, Michael Petrov, and Chris Olah. Curve detectors. *Distill*, 5(6):e00024–003, 2020.

Yuan Cao, Zixiang Chen, Misha Belkin, and Quanquan Gu. Benign overfitting in two-layer convolutional neural networks. *Advances in neural information processing systems*, 35:25237–25250, 2022.

Bo Chen, Xiaoyu Li, Yingyu Liang, Zhenmei Shi, and Zhao Song. Bypassing the exponential dependency: Looped transformers efficiently learn in-context by multi-step gradient descent. *arXiv preprint arXiv:2410.11268*, 2024.

Bo Chen, Xiaoyu Li, Yingyu Liang, Zhenmei Shi, and Zhao Song. Bypassing the exponential dependency: Looped transformers efficiently learn in-context by multi-step gradient descent. In *International Conference on Artificial Intelligence and Statistics*, 2025.

Sitan Chen, Jerry Li, and Zhao Song. Learning mixtures of linear regressions in subexponential time via fourier moments. In *Proceedings of the 52nd Annual ACM SIGACT Symposium on Theory of Computing*, pages 587–600, 2020.

Xiang Chen, Zhao Song, Baocheng Sun, Junze Yin, and Danyang Zhuo. Query complexity of active learning for function family with nearly orthogonal basis. *arXiv preprint arXiv:2306.03356*, 2023.

Xue Chen, Daniel M Kane, Eric Price, and Zhao Song. Fourier-sparse interpolation without a frequency gap. In *2016 IEEE 57th Annual Symposium on Foundations of Computer Science (FOCS)*, pages 741–750. IEEE, 2016.

Lenaic Chizat and Francis Bach. Implicit bias of gradient descent for wide two-layer neural networks trained with the logistic loss. In *Conference on Learning Theory*. PMLR, 2020.

Bilal Chughtai, Lawrence Chan, and Neel Nanda. A toy model of universality: Reverse engineering how networks learn group operations. In *International Conference on Machine Learning*, pages 6243–6267. PMLR, 2023.

Alexandru Damian, Jason Lee, and Mahdi Soltanolkotabi. Neural networks can learn representations with gradient descent. In *Conference on Learning Theory*. PMLR, 2022.

Amit Daniely and Eran Malach. Learning parities with neural networks. *Advances in Neural Information Processing Systems*, 33:20356–20365, 2020.

Darshil Doshi, Tianyu He, Aritra Das, and Andrey Gromov. Grokking modular polynomials. *arXiv preprint arXiv:2406.03495*, 2024.

Nelson Elhage, Neel Nanda, Catherine Olsson, Tom Henighan, Nicholas Joseph, Ben Mann, Amanda Askell, Yuntao Bai, Anna Chen, Tom Conerly, et al. A mathematical framework for transformer circuits. *Transformer Circuits Thread*, 1, 2021.

Nelson Elhage, Tristan Hume, Catherine Olsson, Nicholas Schiefer, Tom Henighan, Shauna Kravec, Zac Hatfield-Dodds, Robert Lasenby, Dawn Drain, Carol Chen, et al. Toy models of superposition. *arXiv preprint arXiv:2209.10652*, 2022.

Spencer Frei, Niladri S Chatterji, and Peter Bartlett. Benign overfitting without linearity: Neural network classifiers trained by gradient descent for noisy linear data. In *Conference on Learning Theory*, pages 2668–2703. PMLR, 2022a.

Spencer Frei, Gal Vardi, Peter Bartlett, Nathan Srebro, and Wei Hu. Implicit bias in leaky relu networks trained on high-dimensional data. In *The Eleventh International Conference on Learning Representations*, 2022b.

Spencer Frei, Gal Vardi, Peter Bartlett, and Nathan Srebro. Benign overfitting in linear classifiers and leaky relu networks from kkt conditions for margin maximization. In *The Thirty Sixth Annual Conference on Learning Theory*, pages 3173–3228. PMLR, 2023.

Peng Gao, Chiori Hori, Shijie Geng, Takaaki Hori, and Jonathan Le Roux. Multi-pass transformer for machine translation. *arXiv preprint arXiv:2009.11382*, 2020.

Yeqi Gao, Zhao Song, and Baocheng Sun. An $O(k \log n)$ time fourier set query algorithm. *arXiv preprint arXiv:2208.09634*, 2022.

Andrey Gromov. Grokking modular arithmetic. *arXiv preprint arXiv:2301.02679*, 2023.

Suriya Gunasekar, Jason Lee, Daniel Soudry, and Nathan Srebro. Characterizing implicit bias in terms of optimization geometry. In *International Conference on Machine Learning*, pages 1832–1841. PMLR, 2018a.

Suriya Gunasekar, Jason D Lee, Daniel Soudry, and Nati Srebro. Implicit bias of gradient descent on linear convolutional networks. *Advances in Neural Information Processing Systems*, 31, 2018b.

Michael Hanna, Ollie Liu, and Alexandre Variengien. How does gpt-2 compute greater-than?: Interpreting mathematical abilities in a pre-trained language model. *Advances in Neural Information Processing Systems*, 36, 2023.

Ishay Haviv and Oded Regev. The restricted isometry property of subsampled fourier matrices. In *Geometric aspects of functional analysis*, pages 163–179. Springer, 2017.

Dan Hendrycks, Collin Burns, Saurav Kadavath, Akul Arora, Steven Basart, Eric Tang, Dawn Song, and Jacob Steinhardt. Measuring mathematical problem solving with the math dataset. *arXiv preprint arXiv:2103.03874*, 2021.

Piotr Indyk and Michael Kapralov. Sample-optimal Fourier sampling in any constant dimension. In *IEEE 55th Annual Symposium onFoundations of Computer Science (FOCS)*, pages 514–523. IEEE, 2014.

Piotr Indyk, Michael Kapralov, and Eric Price. (nearly) sample-optimal sparse fourier transform. In *Proceedings of the twenty-fifth annual ACM-SIAM symposium on Discrete algorithms (SODA)*, pages 480–499. SIAM, 2014.

Arthur Jacot. Implicit bias of large depth networks: a notion of rank for nonlinear functions. In *The Eleventh International Conference on Learning Representations*, 2022.

Ziwei Ji and Matus Telgarsky. The implicit bias of gradient descent on nonseparable data. In *Conference on Learning Theory*, pages 1772–1798. PMLR, 2019.

Ziwei Ji and Matus Telgarsky. Directional convergence and alignment in deep learning. *Advances in Neural Information Processing Systems*, 33:17176–17186, 2020.

Albert Q. Jiang, Alexandre Sablayrolles, Arthur Mensch, Chris Bamford, Devendra Singh Chaplot, Diego de las Casas, Florian Bressand, Gianna Lengyel, Guillaume Lample, Lucile Saulnier, Lélio Renard Lavaud, Marie-Anne Lachaux, Pierre Stock, Teven Le Scao, Thibaut Lavril, Thomas Wang, Timothée Lacroix, and William El Sayed. Mistral 7b, 2023.

Yaonan Jin, Daogao Liu, and Zhao Song. Super-resolution and robust sparse continuous fourier transform in any constant dimension: Nearly linear time and sample complexity. In *ACM-SIAM Symposium on Discrete Algorithms (SODA)*, 2023.

Michael Kapralov. Sparse Fourier transform in any constant dimension with nearly-optimal sample complexity in sublinear time. In *Symposium on Theory of Computing Conference (STOC)*, 2016.

Michael Kapralov. Sample efficient estimation and recovery in sparse FFT via isolation on average. In *58th Annual IEEE Symposium on Foundations of Computer Science (FOCS)*, 2017.

Yekun Ke, Xiaoyu Li, Yingyu Liang, Zhenmei Shi, and Zhao Song. Advancing the understanding of fixed point iterations in deep neural networks: A detailed analytical study. *arXiv preprint arXiv:2410.11279*, 2024.

Yekun Ke, Yingyu Liang, Zhenmei Shi, Zhao Song, and Chiwun Yang. Curse of attention: A kernel-based perspective for why transformers fail to generalize on time series forecasting and beyond. In *Conference on Parsimony and Learning*. PMLR, 2025.

Tanishq Kumar, Blake Bordelon, Samuel J Gershman, and Cengiz Pehlevan. Grokking as the transition from lazy to rich training dynamics. *arXiv preprint arXiv:2310.06110*, 2023.

Yin Tat Lee, Zhao Song, and Qiuyi Zhang. Solving empirical risk minimization in the current matrix multiplication time. In *COLT*, 2019.

Aitor Lewkowycz, Anders Andreassen, David Dohan, Ethan Dyer, Henryk Michalewski, Vinay Ramasesh, Ambrose Slone, Cem Anil, Imanol Schlag, Theo Gutman-Solo, et al. Solving quantitative reasoning problems with language models. *Advances in Neural Information Processing Systems*, 35:3843–3857, 2022.

Chenyang Li, Yingyu Liang, Zhenmei Shi, and Zhao Song. Exploring the frontiers of softmax: Provable optimization, applications in diffusion model, and beyond. *manuscript*, 2024a.

Xiaoyu Li, Yingyu Liang, Zhenmei Shi, Zhao Song, and Mingda Wan. Theoretical constraints on the expressive power of rope-based tensor attention transformers. *arXiv preprint arXiv:2412.18040*, 2024b.

Xiaoyu Li, Yingyu Liang, Jiangxuan Long, Zhenmei Shi, Zhao Song, and Zhen Zhuang. Neural algorithmic reasoning for hypergraphs with looped transformers. *arXiv preprint arXiv:2501.10688*, 2025.

Yingyu Liang, Heshan Liu, Zhenmei Shi, Zhao Song, and Junze Yin. Conv-basis: A new paradigm for efficient attention inference and gradient computation in transformers. *manuscript*, 2024a.

Yingyu Liang, Zhizhou Sha, Zhenmei Shi, Zhao Song, and Yufa Zhou. Looped relu mlps may be all you need as practical programmable computers. *arXiv preprint arXiv:2410.09375*, 2024b.

Yingyu Liang, Zhenmei Shi, Zhao Song, and Yufa Zhou. Tensor attention training: Provably efficient learning of higher-order transformers. *arXiv preprint arXiv:2405.16411*, 2024c.

Yingyu Liang, Zhizhou Sha, Zhenmei Shi, Zhao Song, and Yufa Zhou. Looped relu mlps may be all you need as practical programmable computers. In *International Conference on Artificial Intelligence and Statistics*, 2025.

Ziming Liu, Ouail Kitouni, Niklas S Nolte, Eric Michaud, Max Tegmark, and Mike Williams. Towards understanding grokking: An effective theory of representation learning. *Advances in Neural Information Processing Systems*, 35:34651–34663, 2022.

Ilya Loshchilov and Frank Hutter. Decoupled weight decay regularization. In *International Conference on Learning Representations*, 2018.

Renqian Luo, Liai Sun, Yingce Xia, Tao Qin, Sheng Zhang, Hoifung Poon, and Tie-Yan Liu. Biogpt: generative pre-trained transformer for biomedical text generation and mining. *Briefings in Bioinformatics*, 23(6), 2022.

Kaifeng Lyu and Jian Li. Gradient descent maximizes the margin of homogeneous neural networks. In *International Conference on Learning Representations*, 2019.

Kaifeng Lyu, Zhiyuan Li, Runzhe Wang, and Sanjeev Arora. Gradient descent on two-layer nets: Margin maximization and simplicity bias. *Advances in Neural Information Processing Systems*, 34:12978–12991, 2021.

Kaifeng Lyu, Jikai Jin, Zhiyuan Li, Simon S Du, Jason D Lee, and Wei Hu. Dichotomy of early and late phase implicit biases can provably induce grokking. In *The Twelfth International Conference on Learning Representations*, 2024.

Kevin Meng, David Bau, Alex Andonian, and Yonatan Belinkov. Locating and editing factual associations in gpt. *Advances in Neural Information Processing Systems*, 35:17359–17372, 2022.

William Merrill, Nikolaos Tsilivis, and Aman Shukla. A tale of two circuits: Grokking as competition of sparse and dense subnetworks. *arXiv preprint arXiv:2303.11873*, 2023.

Beren Millidge. Grokking'grokking', 2022.

Edward Moroshko, Blake E Woodworth, Suriya Gunasekar, Jason D Lee, Nati Srebro, and Daniel Soudry. Implicit bias in deep linear classification: Initialization scale vs training accuracy. *Advances in Neural Information Processing Systems*, 33, 2020.

Depen Morwani, Benjamin L Edelman, Costin-Andrei Oncescu, Rosie Zhao, and Sham Kakade. Feature emergence via margin maximization: case studies in algebraic tasks. In *The Twelfth International Conference on Learning Representations*, 2024.

Shikhar Murty, Pratyusha Sharma, Jacob Andreas, and Christopher D Manning. Grokking of hierarchical structure in vanilla transformers. *arXiv preprint arXiv:2305.18741*, 2023.

Vasileios Nakos, Zhao Song, and Zhengyu Wang. (nearly) sample-optimal sparse fourier transform in any dimension; ripless and filterless. In *2019 IEEE 60th Annual Symposium on Foundations of*

Computer Science (FOCS), pages 1568–1577. IEEE, 2019.

Neel Nanda, Lawrence Chan, Tom Lieberum, Jess Smith, and Jacob Steinhardt. Progress measures for grokking via mechanistic interpretability. In *The Eleventh International Conference on Learning Representations*, 2023a.

Neel Nanda, Andrew Lee, and Martin Wattenberg. Emergent linear representations in world models of self-supervised sequence models. *arXiv preprint arXiv:2309.00941*, 2023b.

Chris Olah, Nick Cammarata, Ludwig Schubert, Gabriel Goh, Michael Petrov, and Shan Carter. Zoom in: An introduction to circuits. *Distill*, 5(3): e00024–001, 2020.

Catherine Olsson, Nelson Elhage, Neel Nanda, Nicholas Joseph, Nova DasSarma, Tom Henighan, Ben Mann, Amanda Askell, Yuntao Bai, Anna Chen, et al. In-context learning and induction heads. *arXiv preprint arXiv:2209.11895*, 2022.

OpenAI. Gpt-4 technical report, 2023.

Alethea Power, Yuri Burda, Harri Edwards, Igor Babuschkin, and Vedant Misra. Grokking: Generalization beyond overfitting on small algorithmic datasets. *arXiv preprint arXiv:2201.02177*, 2022.

Gabriele Prato, Ella Charlaix, and Mehdi Rezagholizadeh. Fully quantized transformer for machine translation. In *Findings of the Association for Computational Linguistics: EMNLP 2020*, pages 1–14, 2020.

Philip Quirke and Fazl Barez. Understanding addition in transformers. In *The Twelfth International Conference on Learning Representations*, 2023.

Noa Rubin, Inbar Seroussi, and Zohar Ringel. Droplets of good representations: Grokking as a first order phase transition in two layer networks. *arXiv preprint arXiv:2310.03789*, 2023.

Clayton Sanford, Daniel Hsu, and Matus Telgarsky. Representational strengths and limitations of transformers. In *Thirty-seventh Conference on Neural Information Processing Systems*, 2023.

Eshika Saxena, Alberto Alfarano, Emily Wenger, and Kristin Lauter. Teaching transformers modular arithmetic at scale. *arXiv preprint arXiv:2410.03569*, 2024.

David Saxton, Edward Grefenstette, Felix Hill, and Pushmeet Kohli. Analysing mathematical reasoning abilities of neural models. In *International Conference on Learning Representations*, 2018.

Harshay Shah, Kaustav Tamuly, Aditi Raghunathan, Prateek Jain, and Praneeth Netrapalli. The pitfalls of simplicity bias in neural networks. *Advances in Neural Information Processing Systems*, 33:9573–9585, 2020.

Shai Shalev-Shwartz, Ohad Shamir, and Shaked Shammah. Failures of gradient-based deep learning. In *International Conference on Machine Learning*, pages 3067–3075. PMLR, 2017.

Zhenmei Shi, Junyi Wei, and Yingyu Liang. A theoretical analysis on feature learning in neural networks: Emergence from inputs and advantage over fixed features. In *International Conference on Learning Representations*, 2022.

Zhenmei Shi, Jiefeng Chen, Kunyang Li, Jayaram Raghuram, Xi Wu, Yingyu Liang, and Somesh Jha. The trade-off between universality and label efficiency of representations from contrastive learning. In *The Eleventh International Conference on Learning Representations*, 2023a. URL `https://openreview.net/forum?id=rvsbw2YthH_`.

Zhenmei Shi, Yifei Ming, Ying Fan, Frederic Sala, and Yingyu Liang. Domain generalization via nuclear norm regularization. In *Conference on Parsimony and Learning (Proceedings Track)*, 2023b. URL `https://openreview.net/forum?id=hJd66ZzXEZ`.

Zhenmei Shi, Junyi Wei, and Yingyu Liang. Provable guarantees for neural networks via gradient feature learning. *Advances in Neural Information Processing Systems*, 36, 2023c.

Zhenmei Shi, Yifei Ming, Xuan-Phi Nguyen, Yingyu Liang, and Shafiq Joty. Discovering the gems in early layers: Accelerating long-context llms with 1000x input token reduction. *arXiv preprint arXiv:2409.17422*, 2024a.

Zhenmei Shi, Junyi Wei, Zhuoyan Xu, and Yingyu Liang. Why larger language models do in-context learning differently? In *International Conference on Machine Learning*. PMLR, 2024b.

Zhao Song. *Matrix Theory: Optimization, Concentration and Algorithms*. PhD thesis, The University of Texas at Austin, 2019.

Zhao Song, Baocheng Sun, Omri Weinstein, and Ruizhe Zhang. Sparse fourier transform over lattices: A unified approach to signal reconstruction. *arXiv preprint arXiv:2205.00658*, 2022.

Zhao Song, Baocheng Sun, Omri Weinstein, and Ruizhe Zhang. Quartic samples suffice for fourier interpolation. In *2023 IEEE 64th Annual Symposium on Foundations of Computer Science (FOCS)*, pages 1414–1425. IEEE, 2023a.

Zhao Song, Mingquan Ye, Junze Yin, and Lichen Zhang. A nearly-optimal bound for fast regression with ℓ_∞, guarantee. In *ICML*, volume 202 of *Proceedings of Machine Learning Research*, pages 32463–32482. PMLR, 2023b.

Daniel Soudry, Elad Hoffer, Mor Shpigel Nacson, Suriya Gunasekar, and Nathan Srebro. The implicit bias of gradient descent on separable data. *The Journal of Machine Learning Research*, 19(1):2822–2878, 2018.

Dashiell Stander, Qinan Yu, Honglu Fan, and Stella Biderman. Grokking group multiplication with cosets. *arXiv preprint arXiv:2312.06581*, 2023.

Gemini Team, Rohan Anil, Sebastian Borgeaud, Yonghui Wu, Jean-Baptiste Alayrac, Jiahui Yu, Radu Soricut, Johan Schalkwyk, Andrew M Dai, Anja Hauth, et al. Gemini: a family of highly capable multimodal models. *arXiv preprint arXiv:2312.11805*, 2023.

Gemma Team, Thomas Mesnard, Cassidy Hardin, Robert Dadashi, Surya Bhupatiraju, Shreya Pathak, Laurent Sifre, Morgane Rivière, Mihir Sanjay Kale, Juliette Love, et al. Gemma: Open models based on gemini research and technology. *arXiv preprint arXiv:2403.08295*, 2024.

Vimal Thilak, Etai Littwin, Shuangfei Zhai, Omid Saremi, Roni Paiss, and Joshua Susskind. The slingshot mechanism: An empirical study of adaptive optimizers and the grokking phenomenon. *arXiv preprint arXiv:2206.04817*, 2022.

Curt Tigges, Oskar John Hollinsworth, Atticus Geiger, and Neel Nanda. Linear representations of sentiment in large language models. *arXiv preprint arXiv:2310.15154*, 2023.

Alexander Tsigler and Peter L Bartlett. Benign overfitting in ridge regression. *Journal of Machine Learning Research*, 24(123):1–76, 2023.

Gal Vardi. On the implicit bias in deep-learning algorithms. *Communications of the ACM*, 66(6):86–93, 2023.

Vikrant Varma, Rohin Shah, Zachary Kenton, János Kramár, and Ramana Kumar. Explaining grokking through circuit efficiency. *arXiv preprint arXiv:2309.02390*, 2023.

Ashish Vaswani, Noam Shazeer, Niki Parmar, Jakob Uszkoreit, Llion Jones, Aidan N Gomez, Łukasz Kaiser, and Illia Polosukhin. Attention is all you need. *Advances in neural information processing systems*, 30, 2017.

Colin Wei, Jason D Lee, Qiang Liu, and Tengyu Ma. Regularization matters: Generalization and optimization of neural nets vs their induced kernel. *Advances in Neural Information Processing Systems*, 32, 2019a.

Colin Wei, Jason D Lee, Qiang Liu, and Tengyu Ma. Regularization matters: Generalization and optimization of neural nets vs their induced kernel. *Advances in Neural Information Processing Systems*, 32, 2019b.

Jason Wei, Yi Tay, Rishi Bommasani, Colin Raffel, Barret Zoph, Sebastian Borgeaud, Dani Yogatama, Maarten Bosma, Denny Zhou, Donald Metzler, Ed H. Chi, Tatsunori Hashimoto, Oriol Vinyals, Percy Liang, Jeff Dean, and William Fedus. Emergent abilities of large language models. *Transactions on Machine Learning Research*, 2022.

Zhiwei Xu, Yutong Wang, Spencer Frei, Gal Vardi, and Wei Hu. Benign overfitting and grokking in relu networks for xor cluster data. In *The Twelfth International Conference on Learning Representations*, 2024a.

Zhuoyan Xu, Zhenmei Shi, Junyi Wei, Yin Li, and Yingyu Liang. Improving foundation models for few-shot learning via multitask finetuning. In *ICLR 2023 Workshop on Mathematical and Empirical Understanding of Foundation Models*, 2023. URL `https://openreview.net/forum?id=szNb8Hp3d3`.

Zhuoyan Xu, Zhenmei Shi, and Yingyu Liang. Do large language models have compositional ability? an investigation into limitations and scalability. In *ICLR 2024 Workshop on Mathematical and Empirical Understanding of Foundation Models*, 2024b. URL `https://openreview.net/forum?id=4XPeF0SbJs`.

Zhuoyan Xu, Zhenmei Shi, Junyi Wei, Fangzhou Mu, Yin Li, and Yingyu Liang. Towards few-shot adaptation of foundation models via multitask finetuning. In *International Conference on Learning Representations*, 2024c.

Roozbeh Yousefzadeh and Xuenan Cao. Large language models' understanding of math: Source criticism and extrapolation. *arXiv preprint arXiv:2311.07618*, 2023.

Shizhuo Dylan Zhang, Curt Tigges, Stella Biderman, Maxim Raginsky, and Talia Ringer. Can transformers learn to solve problems recursively? *arXiv preprint arXiv:2305.14699*, 2023.

Yifan Zhang, Yifeng Liu, Huizhuo Yuan, Zhen Qin, Yang Yuan, Quanquan Gu, and Andrew Chi-Chih Yao. Tensor product attention is all you need. *arXiv preprint arXiv:2501.06425*, 2025.

Ziqian Zhong, Ziming Liu, Max Tegmark, and Jacob Andreas. The clock and the pizza: Two stories in mechanistic explanation of neural networks. *Advances in Neural Information Processing Systems*, 36, 2023.

Checklist

1. For all models and algorithms presented, check if you include:
   (a) A clear description of the mathematical setting, assumptions, algorithm, and/or model. [Yes]
   (b) An analysis of the properties and complexity (time, space, sample size) of any algorithm. [Yes]
   (c) (Optional) Anonymized source code, with specification of all dependencies, including external libraries. [Not Applicable]

2. For any theoretical claim, check if you include:
   (a) Statements of the full set of assumptions of all theoretical results. [Yes]
   (b) Complete proofs of all theoretical results. [Yes]
   (c) Clear explanations of any assumptions. [Yes]

3. For all figures and tables that present empirical results, check if you include:
   (a) The code, data, and instructions needed to reproduce the main experimental results (either in the supplemental material or as a URL). [Yes]
   (b) All the training details (e.g., data splits, hyperparameters, how they were chosen). [Yes]
   (c) A clear definition of the specific measure or statistics and error bars (e.g., with respect to the random seed after running experiments multiple times). [Yes]
   (d) A description of the computing infrastructure used. (e.g., type of GPUs, internal cluster, or cloud provider). [Yes]

4. If you are using existing assets (e.g., code, data, models) or curating/releasing new assets, check if you include:
   (a) Citations of the creator if your work uses existing assets. [Not Applicable]
   (b) The license information of the assets, if applicable. [Not Applicable]
   (c) New assets either in the supplemental material or as a URL, if applicable. [Not Applicable]
   (d) Information about consent from data providers/curators. [Not Applicable]
   (e) Discussion of sensible content if applicable, e.g., personally identifiable information or offensive content. [Not Applicable]

5. If you used crowdsourcing or conducted research with human subjects, check if you include:
   (a) The full text of instructions given to participants and screenshots. [Not Applicable]
   (b) Descriptions of potential participant risks, with links to Institutional Review Board (IRB) approvals if applicable. [Not Applicable]
   (c) The estimated hourly wage paid to participants and the total amount spent on participant compensation. [Not Applicable]

Fourier Circuits in Neural Networks and Transformers: A Case Study of Modular Arithmetic with Multiple Inputs: Supplementary Materials

Contents

Roadmap. In Section A, we discuss the societal impacts of our work. In Section B, we introduce some definitions that will be used in the proof. In Section C, we introduce some auxiliary lemma from previous work that we need. In Section D, Section E, Section F, Section G, we provide the proof of our Lemmas and our main results. In particular, we provide two versions of proof (1) $k = 3$ and (2) general $k \geq 3$. We use $k = 3$ version to illustrate our proof intuition and then extend our proof to the general k version. Finally, in Section H, we provide more experimental results and implementation details.

A Societal Impact

Our work aims to understand the potential of large language models in mathematical reasoning and modular arithmetic. Our paper is purely theoretical and empirical in nature (mathematics problem) and thus we foresee no immediate negative ethical impact.

We propose that neural networks and transformers prefer to learn Fourier circuits when training on modular addition involving k inputs under SGD, which may have a positive impact on the machine learning community.

We hope our work will inspire effective algorithm design and promote a better understanding of large language models learning mechanisms.

B More Notations and Definitions

We use $\mathbf{i}$ to denote $\sqrt{-1}$. Let $z = a + \mathbf{i}b$ denote a complex number where a and b are real numbers. Then we have $\overline{z} = a - \mathbf{i}b$ and $|z| := \sqrt{a^2 + b^2}$.

For any positive integer n, we use $[n]$ to denote set $\{1, 2, \cdots, n\}$. We use $\mathbb{E}[]$ to denote expectation. We use $\Pr[]$ to denote probability. We use $z^\top$ to denote the transpose of a vector z.

Considering a vector z, we denote the ℓ_2 norm as $\|z\|_2 := (\sum_{i=1}^n z_i^2)^{1/2}$. We denote the ℓ_1 norm as $\|z\|_1 := \sum_{i=1}^n |z_i|$. The number of non-zero entries in vector z is defined as $\|z\|_0$. $\|z\|_\infty$ is defined as $\max_{i \in [n]} |z_i|$.

We define the vector norm and matrix norm as the following.

Definition B.1 (L_b (vector) norm)**.** *Given a vector $v \in \mathbb{R}^n$ and $b \geq 1$, we have $\|v\|_b := (\sum_{i=1}^n |v_i|^b)^{1/b}$.*

Definition B.2 ($L_{a,b}$ (matrix) norm)**.** *The $L_{a,b}$ norm of a network with parameters $\theta = \{\theta_i\}_{i=1}^m$ is $\|\theta\|_{a,b} := (\sum_{i=1}^m \|\theta_i\|_a^b)^{1/b}$, where θ_i denotes the vector of concatenated parameters for a single neuron.*

We define our regularized training objective function.

Definition B.3. *Let l be the cross-entropy loss. Our regularized training objective function is*

$$\mathcal{L}_\lambda(\theta) := \frac{1}{|D_p|} \sum_{(x,y) \in D_p} l(f(\theta, x), y) + \lambda \|\theta\|_{2,k+1}.$$

Definition B.4. *We define $\Theta^* := \arg\max_{\theta \in \Theta} h(\theta)$.*

Finally, let $\Omega := \mathbb{R}^{p \times (k+1)}$ denote the domain of each θ_i, and let Ω' be a subset of Ω. We say the parameter set $\theta = \{\theta_1, \ldots, \theta_m\}$ has directional support on Ω', if for every $i \in [m]$, either $\theta_i = 0$ or there exists $\alpha_i > 0$ such that $\alpha_i \theta_i \in \Omega'$.

C Tools from Previous Work

Section C.1 states that we can use the single neuron level optimization to get the maximum-margin network. Section C.2 introduces the maximum-margin for multi-class.

C.1 Tools from Previous Work: Implying Single/Combined Neurons

Lemma C.1 (Lemma 5 in page 8 in Morwani et al. (2024))**.** *If the following conditions hold*

- *Given $\Theta := \{\theta : \|\theta\|_{a,b} \leq 1\}$.*
- *Given $\Theta_q'^* := \arg\max_{\theta \in \Theta} \mathbb{E}_{(x,y) \sim q}[g'(\theta, x, y)]$.*
- *Given $\Omega := \{\theta_i : \|\theta_i\|_a \leq 1\}$.*
- *Given $\Omega_q'^* := \arg\max_{\theta_i \in \Omega} \mathbb{E}_{(x,y) \sim q}[\psi'(\theta, x, y)]$.*

Then:

- *Let $\theta \in \Theta_q'^*$. We have θ only has directional support on $\Omega_q'^*$.*
- *Given $\theta_1^*, \ldots, \theta_m^* \in \Omega_q'^*$, we have for any set of neuron scalars where $\sum_{i=1}^m \alpha_i^\nu = 1, \alpha_i \geq 0$, the weights $\theta = \{\alpha_i \theta_i^*\}_{i=1}^m$ is in $\Theta_q'^*$.*

Given q^*, then we can get the θ^* satisfying

$$\theta^* \in \arg\min_{\theta \in \Theta} \mathop{\mathbb{E}}_{(x,y) \sim q^*} [g'(\theta, x, y)]. \tag{6}$$

C.2 Tools from Previous Work: Maximum Margin for Multi-Class

Lemma C.2 (Lemma 6 in page 8 in Morwani et al. (2024))**.** *If the following conditions hold*

- *Given* $\Theta = \{\theta : \|\theta\|_{a,b} \leq 1\}$ *and* $\Theta'^{*}_{q} = \arg\max_{\theta \in \Theta} \mathbb{E}_{(x,y)\sim q}[g'(\theta, x, y)]$.
- *Given* $\Omega = \{\theta_i : \|\theta_i\|_a \leq 1\}$ *and* $\Omega'^{*}_{q} = \arg\max_{\theta_i \in \Omega} \mathbb{E}_{(x,y)\sim q}[\psi'(\theta, x, y)]$.
- *Suppose that* $\exists\{\theta^*, q^*\}$ *such that Equations* (4) *and* (6)*, and 3.8 holds.*

Then, we can show:

- $\theta^* \in \arg\max_{\theta \in \Theta} g(\theta, x, y)$
- $\forall \widehat{\theta} \in \arg\max_{\theta \in \Theta} \min_{(x,y)\in D} g(\theta, x, y)$ *the below properties hold:*
  - $\widehat{\theta}$ *only has directional support on* $\Omega'^{*}_{q^*}$.
  - $\forall (x,y) \in \mathrm{spt}(q^*), f(\widehat{\theta}, x, y) - \max_{y' \in \mathcal{Y}\backslash\{y\}} f(\widehat{\theta}, x, y') = \gamma^*$.

Condition C.3 (Condition C.1 in page 8 in Morwani et al. (2024))**.** *We have* $g'(\theta^*, x, y) = g(\theta^*, x, y)$ *for all* $(x,y) \in \mathrm{spt}(q^*)$*, where* spt *is the support. It means:* $\{y' \in \mathcal{Y}\backslash\{y\} : \tau(x,y)[y'] > 0\} \subseteq \underset{y' \in \mathcal{Y}\backslash\{y\}}{\arg\max} f(\theta^*, x)[y']$.

D Class-weighted Max-margin Solution of Single Neuron

Section D.1 introduces some definitions. Section D.2 shows how we transfer the problem to discrete Fourier space. Section D.3 proposes the weighted margin of the single neuron. Section D.4 shows how we transfer the problem to discrete Fourier space for general k version. Section D.5 provides the solution set for general k version and the maximum weighted margin for a single neuron.

D.1 Definitions

Definition D.1. *When* $k = 3$*, let*

$$\eta_{u_1,u_2,u_3,w}(\delta) := \mathop{\mathbb{E}}_{a_1,a_2,a_3}[(u_1(a_1) + u_2(a_2) + u_3(a_3))^3 w(a_1 + a_2 + a_3 - \delta)].$$

Definition D.2. *Let* η *be defined in Definition D.1. When* $k = 3$*, provided the following conditions are met*

- *We denote* $\mathcal{B}$ *as the ball that* $\|u_1\|^2 + \|u_2\|^2 + \|u_3\|^2 + \|w\|^2 \leq 1$.

We define

$$\Omega'^{*}_{q} = \underset{u_1,u_2,u_3,w \in \mathcal{B}}{\arg\max} (\eta_{u_1,u_2,u_3,w}(0) - \mathop{\mathbb{E}}_{\delta \neq 0}[\eta_{u_1,u_2,u_3,w}(\delta)]).$$

D.2 Transfer to Discrete Fourier Space

The goal of this section is to prove the following Lemma,

Lemma D.3. *When* $k = 3$*, provided the following conditions are met*

- *We denote* $\mathcal{B}$ *as the ball that* $\|u_1\|^2 + \|u_2\|^2 + \|u_3\|^2 + \|w\|^2 \leq 1$.
- *We define* Ω'^{*}_{q} *in Definition D.2.*
- *We adopt the uniform class weighting:* $\forall c' \neq a_1 + a_2 + a_3, \quad \tau(a_1, a_2, a_3)[c'] := 1/(p-1)$.

We have the following

$$\Omega_q'^* = \arg\max_{u_1,u_2,u_3,,w \in \mathcal{B}} \frac{6}{(p-1)p^3} \sum_{j \neq 0} \widehat{u}_1(j)\widehat{u}_2(j)\widehat{u}_3(j)\widehat{w}(-j).$$

Proof. We have

$$\begin{aligned}
\eta_{u_1,u_2,u_3,w}(\delta) = & \mathop{\mathbb{E}}_{a_1,a_2,a_3}[(u_1(a_1)+u_2(a_2)+u_3(a_3))^3 w(a_1+a_2+a_3-\delta)] \\
= & \mathop{\mathbb{E}}_{a_1,a_2,a_3}[(u_1(a_1)^3 + 3u_1(a_1)^2u_2(a_2) + 3u_1(a_1)^2u_3(a_3) + 3u_1(a_1)u_2(a_2)^2 \\
& + 6u_1(a_1)u_2(a_2)u_3(a_3) + 3u_1(a_1)u_3(a_3)^2 + u_2(a_2)^3 + 3u_2(a_2)^2u_3(a_3) \\
& + 3u_2(a_2)u_3(a_3)^2 + u_3(a_3)^3)w(a_1+a_2+a_3-\delta)].
\end{aligned}$$

Recall $\mathcal{B}$ is defined as Lemma Statement.

The goal is to solve the following mean margin maximization problem:

$$\begin{aligned}
& \arg\max_{u_1,u_2,u_3,w \in \mathcal{B}} (\eta_{u_1,u_2,u_3,w}(0) - \mathop{\mathbb{E}}_{\delta \neq 0}[\eta_{u_1,u_2,u_3,w}(\delta)]) \\
= & \frac{p}{p-1}(\eta_{u_1,u_2,u_3,w}(0) - \mathop{\mathbb{E}}_{\delta}[\eta_{u_1,u_2,u_3,w}(\delta)]),
\end{aligned} \tag{7}$$

where the equation follows $\tau(a_1,a_2,a_3)[c'] := 1/(p-1) \ \ \forall c' \neq a_1+a_2+a_3$ and $1 - \frac{1}{p-1} = \frac{p}{p-1}$.

First, note that

$$\begin{aligned}
& \mathop{\mathbb{E}}_{a_1,a_2,a_3}[u_1(a_1)^3 w(a_1+a_2+a_3-\delta)] \\
= & \mathop{\mathbb{E}}_{a_1}[u_1(a_1)^3 \mathop{\mathbb{E}}_{a_2,a_3}[w(a_1+a_2+a_3-\delta)]] \\
= & 0,
\end{aligned}$$

where the first step follows from taking out the $u_1(a_1)$ from the expectation for a_2, a_3, and the last step is from the definition of w.

Similarly for the $u_2(a_2)^3$,$u_3(a_3)^3$ components of η, they equal to 0.

Note that

$$\begin{aligned}
& \mathop{\mathbb{E}}_{a_1,a_2,a_3}[u_1(a_1)^2 u_2(a_2) w(a_1+a_2+a_3-\delta)] \\
= & \mathop{\mathbb{E}}_{a_1}[u_1(a_1)^2 \mathop{\mathbb{E}}_{a_2}[u_2(a_2) \mathop{\mathbb{E}}_{a_3}[w(a_1+a_2+a_3-\delta)]]] \\
= & 0,
\end{aligned}$$

where the first step follows from simple algebra and the last step comes from the definition of w.

Similarly for the $u_1(a_1)^2u_3(a_3)$, $u_2(a_2)^2u_1(a_1)$, $u_2(a_2)^2u_3(a_3)$, $u_3(a_3)^2u_1(a_1)$, $u_3(a_3)^2u_2(a_2)$ components of η, they equal to 0.

Hence, we can rewrite Eq. (7) as

$$\arg\max_{u_1,u_2,u_3,w \in \mathcal{B}} \frac{6p}{p-1}(\widetilde{\eta}_{u_1,u_2,u_3,w}(0) - \mathop{\mathbb{E}}_{\delta}[\widetilde{\eta}_{u_1,u_2,u_3,w}(\delta)]),$$

where

$$\widetilde{\eta}_{u_1,u_2,u_3,w}(\delta) := \mathop{\mathbb{E}}_{a_1,a_2,a_3}[u_1(a_1)u_2(a_2)u_3(a_3)w(a_1+a_2+a_3-\delta)].$$

Let $\rho := e^{2\pi \mathbf{i}/p}$, and let $\widehat{u}_1, \widehat{u}_2, \widehat{u}_3, \widehat{w}$ be the DFT of u_1, u_2, u_3, and w respectively:

$$\begin{aligned}
& \widetilde{\eta}_{u_1,u_2,u_3,w}(\delta) \\
= & \mathop{\mathbb{E}}_{a_1,a_2,a_3}[(\frac{1}{p}\sum_{j_1=0}^{p-1}\widehat{u}_1(j_1)\rho^{j_1 a_1})(\frac{1}{p}\sum_{j_2=0}^{p-1}\widehat{u}_2(j_2)\rho^{j_2 a_2})(\frac{1}{p}\sum_{j_3=0}^{p-1}\widehat{u}_3(j_3)\rho^{j_3 a_3})(\frac{1}{p}\sum_{j_4=0}^{p-1}\widehat{w}(j_4)\rho^{j_4(a_1+a_2+a_3-\delta)})] \\
= & \frac{1}{p^4}\sum_{j_1,j_2,j_3,j_4}\widehat{u}_1(j_1)\widehat{u}_2(j_2)\widehat{u}_3(j_3)\widehat{w}(j_4)\rho^{-j_4\delta}(\mathop{\mathbb{E}}_{a_1}[\rho^{(j_1+j_4)a_1}])(\mathop{\mathbb{E}}_{a_2}[\rho^{(j_2+j_4)a_2}])(\mathop{\mathbb{E}}_{a_3}[\rho^{(j_3+j_4)a_3}]) \\
= & \frac{1}{p^4}\sum_{j}\widehat{u}_1(j)\widehat{u}_2(j)\widehat{u}_3(j)\widehat{w}(-j)\rho^{j\delta}
\end{aligned}$$

where the first step follows from $\rho := e^{2\pi \mathbf{i}/p}$ and $\widehat{u}_1, \widehat{u}_2, \widehat{u}_3, \widehat{w}$ are the discrete Fourier transforms of u_1, u_2, u_3, w, the second step comes from simple algebra, the last step is from that only terms where $j_1+j_4 = j_2+j_4 = j_3+j_4 = 0$ survive.

Hence, we need to maximize

$$\begin{aligned}
& \frac{6p}{p-1}(\widetilde{\eta}_{u_1,u_2,u_3,w}(0) - \mathop{\mathbb{E}}_{\delta}[\widetilde{\eta}_{u_1,u_2,u_3,w}(\delta)]) \\
= & \frac{6p}{p-1}(\frac{1}{p^4}\sum_{j}\widehat{u}_1(j)\widehat{u}_2(j)\widehat{u}_3(j)\widehat{w}(-j) - \frac{1}{p^4}\sum_{j}\widehat{u}_1(j)\widehat{u}_2(j)\widehat{u}_3(j)\widehat{w}(-j)(\mathop{\mathbb{E}}_{\delta}\rho^{j\delta})) \\
= & \frac{6}{(p-1)p^3}\sum_{j\neq 0}\widehat{u}_1(j)\widehat{u}_2(j)\widehat{u}_3(j)\widehat{w}(-j). \\
= & \frac{6}{(p-1)p^3}\sum_{j\in[-(p-1)/2,+(p-1)/2]\setminus 0}\widehat{u}_1(j)\widehat{u}_2(j)\widehat{u}_3(j)\widehat{w}(-j). \qquad (8)
\end{aligned}$$

where the first step is from $\widetilde{\eta}_{u_1,u_2,u_3,w}(\delta)$ definition, the second step is from $\mathbb{E}_\delta \rho^{j\delta} = 0$ when $j \neq 0$, and the last step follows from simple algebra.

□

D.3 Get Solution Set

Lemma D.4. *When $k = 3$, provided the following conditions are met*

- *We denote $\mathcal{B}$ as the ball that $\|u_1\|^2 + \|u_2\|^2 + \|u_3\|^2 + \|w\|^2 \leq 1$.*
- *We define $\Omega_q'^*$ in Definition D.2.*
- *We adopt the uniform class weighting: $\forall c' \neq a_1 + a_2 + a_3, \quad \tau(a_1, a_2, a_3)[c'] := 1/(p-1)$.*
- *For any $\zeta \in \{1, \ldots, \frac{p-1}{2}\}$, there exists a scaling constant $\beta \in \mathbb{R}$ and*

$$\begin{aligned}
u_1(a_1) &= \beta \cdot \cos(\theta_{u_1}^* + 2\pi\zeta a_1/p) \\
u_2(a_2) &= \beta \cdot \cos(\theta_{u_2}^* + 2\pi\zeta a_2/p) \\
u_3(a_3) &= \beta \cdot \cos(\theta_{u_3}^* + 2\pi\zeta a_3/p) \\
w(c) &= \beta \cdot \cos(\theta_{w}^* + 2\pi\zeta c/p)
\end{aligned}$$

where $\theta_{u_1}^*, \theta_{u_2}^*, \theta_{u_3}^*, \theta_w^* \in \mathbb{R}$ are some phase offsets satisfying $\theta_{u_1}^* + \theta_{u_2}^* + \theta_{u_3}^* = \theta_w^*$.

Then, we have the following

$$\Omega_q'^* = \{(u_1, u_2, u_3, w)\},$$

and

$$\max_{u_1,u_2,u_3,w\in\mathcal{B}}(\eta_{u_1,u_2,u_3,w}(0) - \mathop{\mathbb{E}}_{\delta\neq 0}[\eta_{u_1,u_2,u_3,w}(\delta)]) = \frac{3}{16}\cdot\frac{1}{p(p-1)}.$$

Proof. By Lemma D.3, we only need to maximize Equation (8).

Thus, the mass of $\widehat{u}_1, \widehat{u}_2, \widehat{u}_3$, and $\widehat{w}$ must be concentrated on the same frequencies. For all $j \in \mathbb{Z}_p$, we have

$$\widehat{u}_1(-j) = \overline{\widehat{u}_1(j)}, \widehat{u}_2(-j) = \overline{\widehat{u}_2(j)}, \widehat{u}_3(-j) = \overline{\widehat{u}_3(j)}, \widehat{w}(-j) = \overline{\widehat{w}(j)} \tag{9}$$

as u_1, u_2, u_3, w are real-valued.

For all $j \in \mathbb{Z}_p$ and for u_1, u_2, u_3, w, we denote $\theta_{u_1}, \theta_{u_2}, \theta_{u_3}, \theta_w \in [0, 2\pi)^p$ as their phase, e.g.:

$$\widehat{u}_1(j) = |\widehat{u}_1(j)| \exp(\mathbf{i}\theta_{u_1}(j)).$$

Consider the odd p, Equation (8) becomes:

$$\begin{aligned}
(8) =& \frac{6}{(p-1)p^3} \sum_{j \in [-(p-1)/2, +(p-1)/2] \backslash 0} \widehat{u}_1(j)\widehat{u}_2(j)\widehat{u}_3(j)\widehat{w}(-j) \\
=& \frac{6}{(p-1)p^3} \sum_{j=1}^{(p-1)/2} (\widehat{u}_1(j)\widehat{u}_2(j)\widehat{u}_3(j)\overline{\widehat{w}(j)} + \overline{\widehat{u}_1(j)\widehat{u}_2(j)\widehat{u}_3(j)}\widehat{w}(j)) \\
=& \frac{6}{(p-1)p^3} \sum_{j=1}^{(p-1)/2} |\widehat{u}_1(j)||\widehat{u}_2(j)||\widehat{u}_3(j)||\widehat{w}(j)| \cdot \\
& \big(\exp(\mathbf{i}(\theta_{u_1}(j) + \theta_{u_2}(j) + \theta_{u_3}(j) - \theta_w(j)) + \exp(\mathbf{i}(-\theta_{u_1}(j) - \theta_{u_2}(j) - \theta_{u_3}(j) + \theta_w(j))\big) \\
=& \frac{12}{(p-1)p^3} \sum_{j=1}^{(p-1)/2} |\widehat{u}_1(j)||\widehat{u}_2(j)||\widehat{u}_3(j)||\widehat{w}(j)| \cos(\theta_{u_1}(j) + \theta_{u_2}(j) + \theta_{u_3}(j) - \theta_w(j)).
\end{aligned}$$

where the first step comes from definition (8), the second step follows from Eq. (9), the third step comes from $\widehat{u}_1(-j) = \overline{\widehat{u}_1(j)}$ and $\widehat{u}_1(j) = |\widehat{u}_1(j)| \exp(\mathbf{i}\theta_{u_1}(j))$, the last step follow from Euler's formula.

Thus, we need to optimize:

$$\max_{u_1, u_2, u_3, w \in \mathcal{B}} \frac{12}{(p-1)p^3} \sum_{j=1}^{(p-1)/2} |\widehat{u}_1(j)||\widehat{u}_2(j)||\widehat{u}_3(j)||\widehat{w}(j)| \cos(\theta_{u_1}(j) + \theta_{u_2}(j) + \theta_{u_3}(j) - \theta_w(j)). \tag{10}$$

The norm constraint $\|u_1\|^2 + \|u_2\|^2 + \|u_3\|^2 + \|w\|^2 \le 1$ is equivalent to

$$\|\widehat{u}_1\|^2 + \|\widehat{u}_2\|^2 + \|\widehat{u}_3\|^2 + \|\widehat{w}\|^2 \le p$$

by using Plancherel's theorem. Thus, we need to select them in such a way that

$$\theta_{u_1}(j) + \theta_{u_2}(j) + \theta_{u_3}(j) = \theta_w(j),$$

ensuring that, for each j, the expression $\cos(\theta_{u_1}(j) + \theta_{u_2}(j) + \theta_{u_3}(j) - \theta_w(j)) = 1$ is maximized, except in cases where the scalar of the j-th term is 0.

This further simplifies the problem to:

$$\max_{|\widehat{u}_1|, |\widehat{u}_2|, |\widehat{u}_3|, |\widehat{w}| : \|\widehat{u}_1\|^2 + \|\widehat{u}_2\|^2 + \|\widehat{u}_3\|^2 + \|\widehat{w}\|^2 \le p} \frac{12}{(p-1)p^3} \sum_{j=1}^{(p-1)/2} |\widehat{u}_1(j)||\widehat{u}_2(j)||\widehat{u}_3(j)||\widehat{w}(j)|. \tag{11}$$

Then, we have

$$|\widehat{u}_1(j)||\widehat{u}_2(j)||\widehat{u}_3(j)||\widehat{w}(j)| \le (\frac{1}{4} \cdot (|\widehat{u}_1(j)|^2 + |\widehat{u}_2(j)|^2 + |\widehat{u}_3(j)|^2 + |\widehat{w}(j)|^2))^2. \tag{12}$$

where the first step is from inequality of quadratic and geometric means.

We define $z : \{1, \dots, \frac{p-1}{2}\} \to \mathbb{R}$ as

$$z(j) := |\widehat{u}_1(j)|^2 + |\widehat{u}_2(j)|^2 + |\widehat{u}_3(j)|^2 + |\widehat{w}(j)|^2.$$

We need to have $\widehat{u}_1(0) = \widehat{u}_2(0) = \widehat{u}_3(0) = \widehat{w}(0) = 0$. Then, the upper-bound of Eq. (11) is given by

$$\begin{aligned} & \frac{12}{(p-1)p^3} \cdot \max_{\|z\|_1 \le \frac{p}{2}} \sum_{j=1}^{(p-1)/2} (\frac{z(j)}{4})^2 \\ = & \frac{3}{4(p-1)p^3} \cdot \max_{\|z\|_1 \le \frac{p}{2}} \sum_{j=1}^{(p-1)/2} z(j)^2 \\ = & \frac{3}{4(p-1)p^3} \cdot \max_{\|z\|_1 \le \frac{p}{2}} \|z\|_2^2 \\ \le & \frac{3}{4(p-1)p^3} \cdot \frac{p^2}{4} \\ = & \frac{3}{16} \cdot \frac{1}{p(p-1)}, \end{aligned}$$

where the first step follows from simple algebra, the second step comes from the definition of L_2 norm, the third step follows from $\|z\|_2 \le \|z\|_1 \le \frac{p}{2}$, the last step comes from simple algebra.

For the inequality of quadratic and geometric means, Eq. (12) becomes equality when $|\widehat{u}_1(j)| = |\widehat{u}_2(j)| = |\widehat{u}_3(j)| = |\widehat{w}(j)|$. To achieve $\|z\|_2 = \frac{p}{2}$, all the mass must be placed on a single frequency. Hence, for some frequency $\zeta \in \{1, \dots, \frac{p-1}{2}\}$, to achieve the upper bound, we have:

$$|\widehat{u}_1(j)| = |\widehat{u}_2(j)| = |\widehat{u}_3(j)| = |\widehat{w}(j)| = \begin{cases} \sqrt{p/8} & \text{if } j = \pm\zeta \\ 0 & \text{otherwise} \end{cases}, \tag{13}$$

In this case, Eq. (11) matches the upper bound.

$$\frac{12}{(p-1)p^3} \cdot (\frac{p}{8})^2 = \frac{3}{16} \cdot \frac{1}{p(p-1)},$$

where the first step is by simple algebra. Hence, the maximum-margin is $\frac{3}{16} \cdot \frac{1}{p(p-1)}$.

Let $\theta^*_{u_1} := \theta_{u_1}(\zeta)$. Combining all the results, up to scaling, it is established that all neurons which maximize the expected class-weighted margin conform to the form:

$$\begin{aligned} u_1(a_1) = & \frac{1}{p} \sum_{j=0}^{p-1} \widehat{u}_1(j) \rho^{j a_1} \\ = & \frac{1}{p} \cdot (\widehat{u}_1(\zeta)\rho^{\zeta a_1} + \widehat{u}_1(-\zeta)\rho^{-\zeta a_1}) \\ = & \frac{1}{p} \cdot (\sqrt{\frac{p}{8}} \exp(\mathbf{i}\theta^*_{u_1})\rho^{\zeta a_1} + \sqrt{\frac{p}{8}} \exp(-\mathbf{i}\theta^*_{u_1})\rho^{-\zeta a_1}) \\ = & \sqrt{\frac{1}{2p}} \cos(\theta^*_{u_1} + 2\pi\zeta a_1/p), \end{aligned}$$

where the first step comes from the definition of $u_1(a)$, the second step and third step follow from Eq. (13), the last step follows from Euler's formula.

Similarly,

$$\begin{aligned}u_2(a_2) &= \sqrt{\frac{1}{2p}}\cos(\theta^*_{u_2} + 2\pi\zeta a_2/p)\\ u_3(a_3) &= \sqrt{\frac{1}{2p}}\cos(\theta^*_{u_3} + 2\pi\zeta a_3/p)\\ w(c) &= \sqrt{\frac{1}{2p}}\cos(\theta^*_{w} + 2\pi\zeta c/p),\end{aligned}$$

for some phase offsets $\theta^*_{u_1}, \theta^*_{u_2}, \theta^*_{u_3}, \theta^*_w \in \mathbb{R}$ satisfying $\theta^*_{u_1} + \theta^*_{u_2} + \theta^*_{u_3} = \theta^*_w$ and some $\zeta \in \mathbb{Z}_p \backslash \{0\}$, where u_1, u_2, u_3, and w shares the same ζ.

□

D.4 Transfer to Discrete Fourier Space for General k Version

Definition D.5. *Let*

$$\eta_{u_1,\dots,u_k,w}(\delta) := \mathop{\mathbb{E}}_{a_1,\dots,a_k}[(u_1(a_1) + \cdots + u_k(a_k))^k w(a_1 + \cdots + a_k - \delta)].$$

Definition D.6. *Let η be defined in Definition D.5. Provided the following conditions are met*

- *We denote $\mathcal{B}$ as the ball that $\|u_1\|^2 + \cdots + \|u_k\|^2 + \|w\|^2 \le 1$.*

We define

$$\Omega'^*_q = \mathop{\arg\max}_{u_1,\dots,u_k,w \in \mathcal{B}} (\eta_{u_1,\dots,u_k,w}(0) - \mathop{\mathbb{E}}_{\delta \neq 0}[\eta_{u_1,\dots,u_k,w}(\delta)]).$$

The goal of this section is to prove the following Lemma,

Lemma D.7. *Provided the following conditions are met*

- *Let $\mathcal{B}$ denote the ball that $\|u_1\|^2 + \cdots + \|u_k\|^2 + \|w\|^2 \le 1$.*
- *We define $\Omega_q^{'*}$ in Definition D.6.*
- *We adopt the uniform class weighting: $\forall c' \neq a_1 + \cdots + a_k, \quad \tau(a_1, \dots, a_k)[c'] := 1/(p-1)$.*

We have the following

$$\Omega'^*_q = \mathop{\arg\max}_{u_1,\dots,u_k,w \in \mathcal{B}} \frac{k!}{(p-1)p^k} \sum_{j \neq 0} \widehat{w}(-j) \prod_{i=1}^k \widehat{u}_i(j).$$

Proof. We have

$$\eta_{u_1,\dots,u_k,w}(\delta) = \mathop{\mathbb{E}}_{a_1,\dots,a_k}[(u_1(a_1) + \cdots + u_k(a_k))^k w(a_1 + \cdots + a_k - \delta)].$$

The goal is to solve the following mean margin maximization problem:

$$\begin{aligned}&\mathop{\arg\max}_{u_1,\dots,u_k,w \in \mathcal{B}} (\eta_{u_1,\dots,u_k,w}(0) - \mathop{\mathbb{E}}_{\delta \neq 0}[\eta_{u_1,\dots,u_k,w}(\delta)])\\ = &\frac{p}{p-1}(\eta_{u_1,\dots,u_k,w}(0) - \mathop{\mathbb{E}}_{\delta}[\eta_{u_1,\dots,u_k,w}(\delta)]),\end{aligned} \tag{14}$$

where the equation follows $\tau(a_1, \dots, a_k)[c'] := 1/(p-1) \;\; \forall c' \neq a_1 + \cdots + a_k$ and $1 - \frac{1}{p-1} = \frac{p}{p-1}$.

We note that all terms are zero rather than $w(\cdot) \cdot \prod_{i=1}^{k} u_i(a_i)$.

Hence, we can rewrite Eq. (14) as

$$\arg\max_{u_1,\dots,u_k,w \in \mathcal{B}} \frac{k!p}{p-1} (\widetilde{\eta}_{u_1,\dots,u_k,w}(0) - \mathop{\mathbb{E}}_{\delta}[\widetilde{\eta}_{u_1,\dots,u_k,w}(\delta)]),$$

where

$$\widetilde{\eta}_{u_1,\dots,u_k,w}(\delta) := \mathop{\mathbb{E}}_{a_1,\dots,a_k}[w(a_1 + \dots + a_k - \delta) \prod_{i=1}^{k} u_i(a_i)].$$

Let $\rho := e^{2\pi \mathbf{i}/p}$, and $\widehat{u}_1, \dots, \widehat{u}_k, \widehat{w}$ denote the discrete Fourier transforms of $u_1, \dots, u_k$, and w respectively. We have

$$\widetilde{\eta}_{u_1,\dots,u_k,w}(\delta) = \frac{1}{p^{k+1}} \sum_{j=0}^{p-1} \widehat{w}(-j) \rho^{j\delta} \prod_{i=1}^{k} \widehat{u}_i(j)$$

which comes from $\rho := e^{2\pi \mathbf{i}/p}$ and $\widehat{u}_1, \dots, \widehat{u}_k, \widehat{w}$ are the discrete Fourier transforms of $u_1, \dots, u_k, w$.

Hence, we need to maximize

$$\begin{aligned}
& \frac{k!p}{p-1} (\widetilde{\eta}_{u_1,\dots,u_k,w}(0) - \mathop{\mathbb{E}}_{\delta}[\widetilde{\eta}_{u_1,\dots,u_k,w}(\delta)]) \\
= & \frac{k!p}{p-1} \cdot \left(\frac{1}{p^{k+1}} \sum_{j=0}^{p-1} \widehat{w}(-j) \prod_{i=1}^{k} \widehat{u}_i(j) - \frac{1}{p^{k+1}} \sum_{j=0}^{p-1} \widehat{w}(-j) (\mathop{\mathbb{E}}_{\delta}[\rho^{j\delta}]) \prod_{i=1}^{k} \widehat{u}_i(j) \right) \\
= & \frac{k!}{(p-1)p^k} \sum_{j \neq 0} \widehat{w}(-j) \prod_{i=1}^{k} \widehat{u}_i(j). \\
= & \frac{k!}{(p-1)p^k} \sum_{j \in [-(p-1)/2, +(p-1)/2] \backslash 0} \widehat{w}(-j) \prod_{i=1}^{k} \widehat{u}_i(j). \qquad (15)
\end{aligned}$$

where the first step follows from the definition of $\widetilde{\eta}_{u_1,\dots,u_k,w}(\delta)$, the second step follows from $\mathbb{E}_\delta[\rho^{j\delta}] = 0$ when $j \neq 0$, the last step is from simple algebra.

□

D.5 Get Solution Set for General k Version

Lemma D.8 (Formal version of Lemma 4.2)**.** *Provided the following conditions are met*

- *We denote $\mathcal{B}$ as the ball that $\|u_1\|^2 + \dots + \|u_k\|^2 + \|w\|^2 \leq 1$.*
- *Let $\Omega_q^{'*}$ be defined as Definition D.6.*
- *We adopt the uniform class weighting: $\forall c' \neq a_1 + \dots + a_k, \quad \tau(a_1, \dots, a_k)[c'] := 1/(p-1)$.*
- *For any $\zeta \in \{1, \dots, \frac{p-1}{2}\}$, there exists a scaling constant $\beta \in \mathbb{R}$ and*

$$\begin{aligned}
u_1(a_1) &= \beta \cdot \cos(\theta_{u_1}^* + 2\pi\zeta a_1/p) \\
u_2(a_2) &= \beta \cdot \cos(\theta_{u_2}^* + 2\pi\zeta a_2/p) \\
& \dots
\end{aligned}$$

$$u_k(a_k) = \beta \cdot \cos(\theta^*_{u_k} + 2\pi\zeta a_k/p)$$
$$w(c) = \beta \cdot \cos(\theta^*_w + 2\pi\zeta c/p)$$

where $\theta^*_{u_1}, \dots, \theta^*_{u_k}, \theta^*_w \in \mathbb{R}$ are some phase offsets satisfying $\theta^*_{u_1} + \dots + \theta^*_{u_k} = \theta^*_w$.

Then, we have the following

$$\Omega'^*_q = \{(u_1, \dots, u_k, w)\},$$

and

$$\max_{u_1,\dots,u_k,w\in\mathcal{B}} (\eta_{u_1,\dots,u_k,w}(0) - \mathop{\mathbb{E}}_{\delta\neq 0}[\eta_{u_1,\dots,u_k,w}(\delta)]) = \frac{2(k!)}{(2k+2)^{(k+1)/2}(p-1)p^{(k-1)/2}}.$$

Proof. By Lemma D.7, we only need to maximize Equation (15). Thus, the mass of $\widehat{u}_1, \dots, \widehat{u}_k$, and $\widehat{w}$ must be concentrated on the same frequencies. For all $j \in \mathbb{Z}_p$, we have

$$\widehat{u}_i(-j) = \overline{\widehat{u}_i(j)}, \quad \widehat{w}(-j) = \overline{\widehat{w}(j)} \tag{16}$$

as $u_1, \dots, u_k, w$ are real-valued. For all $j \in \mathbb{Z}_p$ and for u_1, u_2, u_3, w, we denote $\theta_{u_1}, \dots, \theta_{u_k}, \theta_w \in [0, 2\pi)^p$ as their phase, e.g.:

$$\widehat{u}_1(j) = |\widehat{u}_1(j)| \exp(\mathbf{i}\theta_{u_1}(j)). \tag{17}$$

Considering odd p, Equation (15) becomes:

$$\begin{aligned}
(15) = & \frac{k!}{(p-1)p^k} \sum_{j\in[-(p-1)/2,+(p-1)/2]\backslash 0} \widehat{w}(-j) \prod_{i=1}^k \widehat{u}_i(j) \\
= & \frac{k!}{(p-1)p^k} \sum_{j=1}^{(p-1)/2} (\prod_{i=1}^k \widehat{u}_i(j)\overline{\widehat{w}(j)} + \widehat{w}(j) \prod_{i=1}^k \overline{\widehat{u}_i(j)}) \\
= & \frac{2(k!)}{(p-1)p^k} \sum_{j=1}^{(p-1)/2} |\widehat{w}(j)| \cos(\sum_{i=1}^k \theta_{u_i}(j) - \theta_w(j)) \prod_{i=1}^k |\widehat{u}_i(j)|.
\end{aligned}$$

where the first step follows from definition (15), the second step comes from Eq. (16), the last step follows from Eq. (17), i.e., Euler's formula.

Thus, we need to optimize:

$$\max_{u_1,\dots,u_k,w\in\mathcal{B}} \frac{2(k!)}{(p-1)p^k} \sum_{j=1}^{(p-1)/2} |\widehat{w}(j)| \cos(\sum_{i=1}^k \theta_{u_i}(j) - \theta_w(j)) \prod_{i=1}^k |\widehat{u}_i(j)|. \tag{18}$$

We can transfer the norm constraint to

$$\|\widehat{u}_1\|^2 + \dots + \|\widehat{u}_k\|^2 + \|\widehat{w}\|^2 \leq p$$

by using Plancherel's theorem.

Therefore, we need to select them in a such way that $\theta_{u_1}(j) + \dots + \theta_{u_k}(j) = \theta_w(j)$, ensuring that, for each j, the expression $\cos(\theta_{u_1}(j) + \dots + \theta_{u_k}(j) - \theta_w(j)) = 1$ is maximized, except in cases where the scalar of the j-th term is 0.

This further simplifies the problem to:

$$\max_{\|\widehat{u}_1\|^2+\dots+\|\widehat{u}_k\|^2+\|\widehat{w}\|^2\leq p} \frac{2(k!)}{(p-1)p^k} \sum_{j=1}^{(p-1)/2} |\widehat{w}(j)| \prod_{i=1}^k |\widehat{u}_i(j)|. \tag{19}$$

Then, we have

$$|\widehat{w}(j)|\prod_{i=1}^{k}|\widehat{u}_i(j)| \leq (\frac{1}{k+1}\cdot(|\widehat{u}_1(j)|^2+\cdots+|\widehat{u}_k(j)|^2+|\widehat{w}(j)|^2))^{(k+1)/2}. \tag{20}$$

where the first step follows from inequality of quadratic and geometric means.

We define $z:\{1,\ldots,\frac{p-1}{2}\}\to\mathbb{R}$, where

$$z(j) := |\widehat{u}_1(j)|^2+\cdots+|\widehat{u}_k(j)|^2+|\widehat{w}(j)|^2.$$

We need to have $\widehat{u}_1(0)=\cdots=\widehat{u}_k(0)=\widehat{w}(0)=0$. Then, the upper-bound of Equation (19) is given by

$$\begin{aligned}
&\frac{2(k!)}{(p-1)p^k}\cdot\max_{\|z\|_1\leq\frac{p}{2}}\sum_{j=1}^{(p-1)/2}(\frac{z(j)}{k+1})^{(k+1)/2}\\
=&\frac{2(k!)}{(k+1)^{(k+1)/2}(p-1)p^k}\cdot\max_{\|z\|_1\leq\frac{p}{2}}\sum_{j=1}^{(p-1)/2}z(j)^{(k+1)/2}\\
\leq&\frac{2(k!)}{(k+1)^{(k+1)/2}(p-1)p^k}\cdot(p/2)^{(k+1)/2}\\
=&\frac{2(k!)}{(2k+2)^{(k+1)/2}(p-1)p^{(k-1)/2}},
\end{aligned}$$

where the first step follows from simple algebra, the second step comes from the definition of L_2 norm, the third step follows from $\|z\|_2\leq\|z\|_1\leq\frac{p}{2}$, the last step follows from simple algebra.

For the inequality of quadratic and geometric means, Eq. (20) becomes equality when $|\widehat{u}_1(j)|=\cdots=|\widehat{u}_k(j)|=|\widehat{w}(j)|$. To achieve $\|z\|_2=\frac{p}{2}$, all the mass must be placed on a single frequency. Hence, for some frequency $\zeta\in\{1,\ldots,\frac{p-1}{2}\}$, to achieve the upper bound, we have:

$$|\widehat{u}_1(j)|=\cdots=|\widehat{u}_k(j)|=|\widehat{w}(j)|=\begin{cases}\sqrt{\frac{p}{2(k+1)}}, & \text{if } j=\pm\zeta;\\ 0, & \text{otherwise.}\end{cases} \tag{21}$$

In this case, Equation (19) matches the upper bound. Hence, this is the maximum-margin.

Let $\theta_{u_1}^*:=\theta_{u_1}(\zeta)$. Combining all the results, up to scaling, it is established that all neurons which maximize the expected class-weighted margin conform to the form:

$$\begin{aligned}
u_1(a_1)=&\frac{1}{p}\sum_{j=0}^{p-1}\widehat{u}_1(j)\rho^{ja_1}\\
=&\frac{1}{p}\cdot(\widehat{u}_1(\zeta)\rho^{\zeta a_1}+\widehat{u}_1(-\zeta)\rho^{-\zeta a_1})\\
=&\frac{1}{p}\cdot(\sqrt{\frac{p}{2(k+1)}}\exp(\mathbf{i}\theta_{u_1}^*)\rho^{\zeta a_1}+\sqrt{\frac{p}{2(k+1)}}\exp(-\mathbf{i}\theta_{u_1}^*)\rho^{-\zeta a_1})\\
=&\sqrt{\frac{2}{(k+1)p}}\cos(\theta_{u_1}^*+2\pi\zeta a_1/p),
\end{aligned}$$

where the first step comes from the definition of $u_1(a)$, the second step and third step follow from Eq. (21), the last step follows from Eq. (17) i.e., Euler's formula.

We have similar results for other neurons where $\theta_{u_1}^*,\ldots,\theta_{u_k}^*,\theta_w^*\in\mathbb{R}$ satisfying $\theta_{u_1}^*+\cdots+\theta_{u_k}^*=\theta_w^*$ and some $\zeta\in\mathbb{Z}_p\backslash\{0\}$, where $u_1,\ldots,u_k$, and w shares the same ζ.

□

E Construct Max Margin Solution

Section E.1 proposed the sum-to-product identities for k inputs. Section E.2 shows how we construct θ^* when $k = 3$. Section E.3 gives the constructions for θ^* for general k version.

E.1 Sum-to-product Identities

Lemma E.1 (Sum-to-product Identities)**.** *If the following conditions hold*

- *Let $a_1, \ldots, a_k$ denote any k real numbers*

We have

- **Part 1.**

$$2^2 \cdot 2! \cdot a_1 a_2 = (a_1 + a_2)^2 - (a_1 - a_2)^2 - (-a_1 + a_2)^2 + (-a_1 - a_2)^2$$

- **Part 2.**

$$\begin{aligned} 2^3 \cdot 3! \cdot a_1 a_2 a_3 = & (a_1 + a_2 + a_3)^3 - (a_1 + a_2 - a_3)^3 - (a_1 - a_2 + a_3)^3 - (-a_1 + a_2 + a_3)^3 \\ & + (a_1 - a_2 - a_3)^3 + (-a_1 + a_2 - a_3)^3 + (-a_1 - a_2 + a_3)^3 - (-a_1 - a_2 - a_3)^3 \end{aligned}$$

- **Part 3.**

$$2^k \cdot k! \cdot \prod_{i=1}^{k} a_i = \sum_{c \in \{-1,+1\}^k} (-1)^{(k - \sum_{i=1}^{k} c_i)/2} (\sum_{j=1}^{k} c_j a_j)^k.$$

Proof. **Proof of Part 1.**

We define A_1, A_2, A_3, A_4 as follows

$$A_1 := \ (a_1 + a_2)^2, A_2 := \ (a_1 - a_2)^2, A_3 := \ (-a_1 + a_2)^2, A_4 := \ (-a_1 - a_2)^2,$$

For the first term, we have

$$A_1 = a_1^2 + a_2^2 + 2a_1 a_2.$$

For the second term, we have

$$A_2 = a_1^2 + a_2^2 - 2a_1 a_2.$$

For the third term, we have

$$A_3 = a_1^2 + a_2^2 - 2a_1 a_2.$$

For the fourth term, we have

$$A_4 = a_1^2 + a_2^2 + 2a_1 a_2.$$

Putting things together, we have

$$\begin{aligned} (a_1 + a_2)^2 - (a_1 - a_2)^2 - (-a_1 + a_2)^2 + (-a_1 - a_2)^2 = & A_1 - A_2 - A_3 + A_4 \\ = & 8a_1 a_2 \\ = & 2^3 a_1 a_2 \end{aligned}$$

Proof of Part 2.

We define $B_1, B_2, B_3, B_4, B_5, B_6, B_7, B_8$ as follows

$$\begin{aligned}
B_1 &:= (a_1 + a_2 + a_3)^3, \\
B_2 &:= (a_1 + a_2 - a_3)^3, \\
B_3 &:= (a_1 - a_2 + a_3)^3, \\
B_4 &:= (-a_1 + a_2 + a_3)^3, \\
B_5 &:= (a_1 - a_2 - a_3)^3, \\
B_6 &:= (-a_1 + a_2 - a_3)^3, \\
B_7 &:= (-a_1 - a_2 + a_3)^3, \\
B_8 &:= (-a_1 - a_2 - a_3)^3,
\end{aligned}$$

For the first term, we have

$$B_1 = a_1^3 + a_2^3 + a_3^3 + 3a_2a_3^2 + 3a_2a_1^2 + 3a_1a_3^2 + 3a_1a_2^2 + 3a_3a_1^2 + 3a_3a_2^2 + 6a_1a_2a_3.$$

For the second term, we have

$$B_2 = a_1^3 + a_2^3 - a_3^3 + 3a_2a_3^2 + 3a_2a_1^2 + 3a_1a_3^2 + 3a_1a_2^2 - 3a_3a_1^2 - 3a_3a_2^2 - 6a_1a_2a_3.$$

For the third term, we have

$$B_3 = a_1^3 - a_2^3 + a_3^3 - 3a_2a_3^2 - 3a_2a_1^2 + 3a_1a_3^2 + 3a_1a_2^2 + 3a_3a_1^2 + 3a_3a_2^2 - 6a_1a_2a_3.$$

For the fourth term, we have

$$B_4 = -a_1^3 + a_2^3 + a_3^3 + 3a_2a_3^2 + 3a_2a_1^2 - 3a_1a_3^2 - 3a_1a_2^2 + 3a_3a_1^2 + 3a_3a_2^2 - 6a_1a_2a_3.$$

For the fifth term, we have

$$B_5 = a_1^3 - a_2^3 - a_3^3 - 3a_2a_3^2 - 3a_2a_1^2 + 3a_1a_3^2 + 3a_1a_2^2 - 3a_3a_1^2 - 3a_3a_2^2 + 6a_1a_2a_3.$$

For the sixth term, we have

$$B_6 = -a_1^3 + a_2^3 - a_3^3 + 3a_2a_3^2 + 3a_2a_1^2 - 3a_1a_3^2 - 3a_1a_2^2 - 3a_3a_1^2 - 3a_3a_2^2 + 6a_1a_2a_3.$$

For the seventh term, we have

$$B_7 = -a_1^3 - a_2^3 + a_3^3 - 3a_2a_3^2 - 3a_2a_1^2 - 3a_1a_3^2 - 3a_1a_2^2 + 3a_3a_1^2 + 3a_3a_2^2 + 6a_1a_2a_3.$$

For the eighth term, we have

$$B_8 = -a_1^3 - a_2^3 - a_3^3 - 3a_2a_3^2 - 3a_2a_1^2 - 3a_1a_3^2 - 3a_1a_2^2 - 3a_3a_1^2 - 3a_3a_2^2 - 6a_1a_2a_3.$$

Putting things together, we have

$$\begin{aligned}
& (a_1 + a_2 + a_3)^3 - (a_1 + a_2 - a_3)^3 - (a_1 - a_2 + a_3)^3 - (-a_1 + a_2 + a_3)^3 \\
& \quad + (a_1 - a_2 - a_3)^3 + (-a_1 + a_2 - a_3)^3 + (-a_1 - a_2 + a_3)^3 - (-a_1 - a_2 - a_3)^3 \\
= {} & B_1 - B_2 - B_3 - B_4 + B_5 + B_6 + B_7 - B_8 \\
= {} & 48a_1a_2a_3 \\
= {} & 3 \cdot 2^4 a_1a_2a_3
\end{aligned}$$

Proof of Part 3.

$$2^k \cdot k! \cdot \prod_{i=1}^{k} a_i = \sum_{c \in \{-1,+1\}^k} (-1)^{(k-\sum_{i=1}^k c_i)/2} (\sum_{j=1}^{k} c_j a_j)^k.$$

We first let $a_1 = 0$. Then each term on RHS can find a corresponding negative copy of this term. In detail, let c_1 change sign and we have, $(-1)^{(k-c_1-\sum_{i=2}^k c_i)/2}(c_1 \cdot 0 + \sum_{j=2}^k c_j a_j)^k = -(-1)^{(k+c_1-\sum_{i=2}^k c_i)/2}(-c_1 \cdot 0 + \sum_{j=2}^k c_j a_j)^k$. We can find this mapping is always one-to-one and onto mapping with each other. Thus, we have RHS is constant 0 regardless of $a_2, \dots, a_k$. Thus, a_1 is a factor of RHS. By symmetry, $a_2, \dots, a_k$ also are factors of RHS. Since RHS is k-th order, we have RHS= $\alpha \prod_{i=1}^k a_i$ where α is a constant. Take $a_1 = \cdots = a_k = 1$, we have $\alpha = 2^k \cdot k!$ =RHS. Thus, we finish the proof. □

E.2 Constructions for θ^*

Lemma E.2. *When $k = 3$, provided the following conditions are met*

- *We denote $\mathcal{B}$ as the ball that $\|u_1\|^2 + \|u_2\|^2 + \|u_3\|^2 + \|w\|^2 \leq 1$.*
- *We define $\Omega_q^{'*}$ in Definition D.2.*
- *We adopt the uniform class weighting: $\forall c' \neq a_1 + a_2 + a_3, \quad \tau(a_1, a_2, a_3)[c'] := 1/(p-1)$.*
- *Let $\cos_\zeta(x)$ denote $\cos(2\pi\zeta x/p)$*
- *Let $\sin_\zeta(x)$ denote $\sin(2\pi\zeta x/p)$*

Then, we have

- *The maximum $L_{2,4}$-margin solution θ^* will consist of $16(p-1)$ neurons $\theta_i^* \in \Omega_q^{'*}$ to simulate $\frac{p-1}{2}$ type of cosine computation, each cosine computation is uniquely determined a $\zeta \in \{1, \dots, \frac{p-1}{2}\}$. In particular, for each ζ the cosine computation is $\cos_\zeta(a_1 + a_2 + a_3 - c), \forall a_1, a_2, a_3, c \in \mathbb{Z}_p$.*

Proof. Referencing Lemma D.4, we can identify elements within $\Omega_q^{'}$. Our set θ^* will be composed of $16(p-1)$ neurons, including 32 neurons dedicated to each frequency in the range $1, \dots, \frac{p-1}{2}$. Focusing on a specific frequency ζ, for the sake of simplicity, let us use $\cos_\zeta(x)$ to represent $\cos(2\pi\zeta x/p)$ and $\sin_\zeta(x)$ likewise. We note:

$$\begin{aligned}
\cos_\zeta(a_1 + a_2 + a_3 - c) =& \cos_\zeta(a_1 + a_2 + a_3)\cos_\zeta(c) + \sin_\zeta(a_1 + a_2 + a_3)\sin_\zeta(c) \\
=& \cos_\zeta(a_1 + a_2)\cos_\zeta(a_3)\cos_\zeta(c) - \sin_\zeta(a_1 + a_2)\sin_\zeta(a_3)\cos_\zeta(c) \\
& + \sin_\zeta(a_1 + a_2)\cos_\zeta(a_3)\sin_\zeta(c) + \cos_\zeta(a_1 + a_2)\sin_\zeta(a_3)\sin_\zeta(c) \\
=& (\cos_\zeta(a_1)\cos_\zeta(a_2) - \sin_\zeta(a_1)\sin_\zeta(a_2))\cos_\zeta(a_3)\cos_\zeta(c) \\
& - (\sin_\zeta(a_1)\cos_\zeta(a_2) + \cos_\zeta(a_1)\sin_\zeta(a_2))\sin_\zeta(a_3)\cos_\zeta(c) \\
& + (\sin_\zeta(a_1)\cos_\zeta(a_2) + \cos_\zeta(a_1)\sin_\zeta(a_2))\cos_\zeta(a_3)\sin_\zeta(c) \\
& + ((\cos_\zeta(a_1)\cos_\zeta(a_2) - \sin_\zeta(a_1)\sin_\zeta(a_2)))\sin_\zeta(a_3)\sin_\zeta(c) \\
=& \cos_\zeta(a_1)\cos_\zeta(a_2)\cos_\zeta(a_3)\cos_\zeta(c) - \sin_\zeta(a_1)\sin_\zeta(a_2)\cos_\zeta(a_3)\cos_\zeta(c) \\
& - \sin_\zeta(a_1)\cos_\zeta(a_2)\sin_\zeta(a_3)\cos_\zeta(c) - \cos_\zeta(a_1)\sin_\zeta(a_2)\sin_\zeta(a_3)\cos_\zeta(c) \\
& + \sin_\zeta(a_1)\cos_\zeta(a_2)\cos_\zeta(a_3)\sin_\zeta(c) + \cos_\zeta(a_1)\sin_\zeta(a_2)\cos_\zeta(a_3)\sin_\zeta(c) \\
& + \cos_\zeta(a_1)\cos_\zeta(a_2)\sin_\zeta(a_3)\sin_\zeta(c) - \sin_\zeta(a_1)\sin_\zeta(a_2)\sin_\zeta(a_3)\sin_\zeta(c)
\end{aligned} \tag{22}$$

where all steps comes from trigonometric function.

Each of these 8 terms can be implemented by 4 neurons $\phi_1, \phi_2, \cdots, \phi_4$. Consider the first term, $\cos_\zeta(a_1)\cos_\zeta(a_2)\cos_\zeta(a_3)\cos_\zeta(c)$.

For the i-th neuron, we have

$$\phi_i = (u_{i,1}(a_1) + u_{i,2}(a_2) + u_{i,3}(a_3))^3 \cdot w_i(c).$$

By changing $(\theta_{i,j})^*$, we can change the constant factor of $\cos_\zeta(\cdot)$ to be $+\beta$ or $-\beta$. Hence, we can view $u_{i,j}(\cdot), w_i(\cdot)$ as the following:

$$\begin{aligned} u_{i,1}(\cdot) &:= p_{i,1} \cdot \cos_\zeta(\cdot), \\ u_{i,2}(\cdot) &:= p_{i,2} \cdot \cos_\zeta(\cdot), \\ u_{i,3}(\cdot) &:= p_{i,3} \cdot \cos_\zeta(\cdot), \\ w_i(\cdot) &:= p_{i,4} \cdot \cos_\zeta(\cdot) \end{aligned}$$

where $p_{i,j} \in \{-1, 1\}$.

For simplicity, let d_i denote $\cos_\zeta(a_i)$.

We set $(\theta^*_{u_1}, \theta^*_{u_2}, \theta^*_{u_3}, \theta^*_w) = (0, 0, 0, 0)$, then

$$p_{1,1}, p_{1,2}, p_{1,3}, p_{1,4} = 1,$$

then we have

$$\phi_1 = (d_1 + d_2 + d_3)^3 \cos_\zeta(c).$$

We set $(\theta^*_{u_1}, \theta^*_{u_2}, \theta^*_{u_3}, \theta^*_w) = (0, 0, \pi, \pi)$, then $p_{2,1}, p_{2,2} = 1$ and $p_{2,3}, p_{2,4} = -1$, then we have

$$\phi_2 = -(d_1 + d_2 - d_3)^3 \cos_\zeta(c).$$

We set $(\theta^*_{u_1}, \theta^*_{u_2}, \theta^*_{u_3}, \theta^*_w) = (0, \pi, 0, \pi)$, then $p_{3,1}, p_{3,3} = 1$ and $p_{3,2}, p_{3,4} = -1$, then we have

$$\phi_3 = -(d_1 - d_2 + d_3)^3 \cos_\zeta(c).$$

We set $(\theta^*_{u_1}, \theta^*_{u_2}, \theta^*_{u_3}, \theta^*_w) = (\pi, 0, 0, \pi)$, then $p_{4,1}, p_{4,4} = -1$ and $p_{2,2}, p_{2,3} = 1$, then we have

$$\phi_4 = -(-d_1 + d_2 + d_3)^3 \cos_\zeta(c).$$

Putting them together, we have

$$\begin{aligned} & \sum_{i=1}^{4} \phi_i(a_1, a_2, a_3) \\ = & \sum_{i=1}^{4} (u_{i,1}(a_1) + u_{i,2}(a_2) + u_{i,3}(a_3))^3 w_i(c) \\ = & \sum_{i=1}^{4} (p_{i,1} \cos_\zeta(a_1) + p_{i,2} \cos_\zeta(a_2) + p_{i,3} \cos_\zeta(a_3))^3 w_i(c) \\ = & [(d_1 + d_2 + d_3)^3 - (d_1 + d_2 - d_3)^3 - (d_1 - d_2 + d_3)^3 - (-d_1 + d_2 + d_3)^3] \cos_\zeta(c) \\ = & 24 d_1 d_2 d_3 \cos_\zeta(c) \\ = & 24 \cos_\zeta(a_1) \cos_\zeta(a_2) \cos_\zeta(a_3) \cos_\zeta(c) \end{aligned} \tag{23}$$

where the first step comes from the definition of ϕ_i, the second step comes from the definition of $u_{i,j}$, the third step comes from $d_i = \cos_\zeta(a_i)$, the fourth step comes from simple algebra, the last step comes from $d_i = \cos_\zeta(a_i)$.

Similarly, consider $-\sin_\zeta(a_1) \sin_\zeta(a_2) \cos_\zeta(a_3) \cos_\zeta(c)$.

We set $(\theta^*_{u_1}, \theta^*_{u_2}, \theta^*_{u_3}, \theta^*_w) = (\pi/2, \pi/2, 0, \pi)$, then we have

$$\phi_1 = -(\sin_\zeta(a_1) + \sin_\zeta(a_2) + \cos_\zeta(a_3))^3 \cos_\zeta(c).$$

We set $(\theta^*_{u_1}, \theta^*_{u_2}, \theta^*_{u_3}, \theta^*_w) = (\pi/2, \pi/2, -\pi, 0)$, then we have

$$\phi_2 = (\sin_\zeta(a_1) + \sin_\zeta(a_2) - \cos_\zeta(a_3))^3 \cos_\zeta(c).$$

We set $(\theta^*_{u_1}, \theta^*_{u_2}, \theta^*_{u_3}, \theta^*_w) = (\pi/2, -\pi/2, 0, 0)$, then we have

$$\phi_3 = (\sin_\zeta(a_1) - \sin_\zeta(a_2) + \cos_\zeta(a_3))^3 \cos_\zeta(c).$$

We set $(\theta^*_{u_1}, \theta^*_{u_2}, \theta^*_{u_3}, \theta^*_w) = (-\pi/2, \pi/2, 0, 0)$, then we have

$$\phi_4 = (-\sin_\zeta(a_1) + \sin_\zeta(a_2) + \cos_\zeta(a_3))^3 \cos_\zeta(c).$$

Putting them together, we have

$$\begin{aligned} & \sum_{i=1}^{4} \phi_i(a_1, a_2, a_3) \\ = & -24 \sin_\zeta(a_1) \sin_\zeta(a_2) \cos_\zeta(a_3) \cos_\zeta(c) \end{aligned} \tag{24}$$

Similarly, all other six terms in Eq. (22) can be composed by four neurons with different $(\theta^*_{u_1}, \theta^*_{u_2}, \theta^*_{u_3}, \theta^*_w)$.

When we include such 56 neurons for all frequencies $\zeta \in \{1, \ldots, \frac{p-1}{2}\}$, we have that the network will calculate the following function

$$\begin{aligned} f(a_1, a_2, a_3, c) = & \sum_{\zeta=1}^{(p-1)/2} \cos_\zeta(a_1 + a_2 + a_3 - c) \\ = & \sum_{\zeta=1}^{p-1} \frac{1}{2} \cdot \exp(2\pi \mathbf{i} \zeta (a_1 + a_2 + a_3 - c)/p) \\ = & \begin{cases} \frac{p-1}{2} & \text{if } a_1 + a_2 + a_3 = c \\ 0 & \text{otherwise} \end{cases} \end{aligned}$$

where the first step comes from the definition of $f(a_1, a_2, a_3, c)$, the second step comes from Euler's formula, the last step comes from the properties of discrete Fourier transform.

The scaling factor β for each neuron can be selected such that the entire network maintains an $L_{2,4}$-norm of 1. In this setup, every data point lies exactly on the margin, meaning $q = \mathrm{unif}(\mathbb{Z}_p)$ uniformly covers points on the margin, thus meeting the criteria for q^* as outlined in Definition 3.5. Furthermore, for any input (a_1, a_2, a_3), the function f yields an identical result across all incorrect labels c', adhering to Condition 3.8. □

E.3 Constructions for θ^* for General k Version

Lemma E.3 (Formal version of Lemma 4.3)**.** *Provided the following conditions are met*

- *We denote $\mathcal{B}$ as the ball that $\|u_1\|^2 + \cdots + \|u_k\|^2 + \|w\|^2 \leq 1$.*
- *We define Ω'^*_q in Definition D.2.*
- *We adopt the uniform class weighting: $\forall c' \neq a_1 + \cdots + a_k, \quad \tau(a_1, \ldots, a_k)[c'] := 1/(p-1)$.*
- *Let $\cos_\zeta(x)$ denote $\cos(2\pi\zeta x/p)$*
- *Let $\sin_\zeta(x)$ denote $\sin(2\pi\zeta x/p)$*

Then, we have

- *The maximum $L_{2,k+1}$-margin solution θ^* will consist of $2^{2k-1} \cdot \frac{p-1}{2}$ neurons $\theta_i^* \in \Omega_q^{'*}$ to simulate $\frac{p-1}{2}$ type of cosine computation, each cosine computation is uniquely determined a $\zeta \in \{1, \dots, \frac{p-1}{2}\}$. In particular, for each ζ the cosine computation is $\cos_\zeta(a_1 + \cdots + a_k - c), \forall a_1, \dots, a_k, c \in \mathbb{Z}_p$.*

Proof. By Lemma D.4, we can get elements of $\Omega_q^{'*}$. Our set θ^* will be composed of $2^{2k-1} \cdot \frac{p-1}{2}$ neurons, including 2^{2k-1} neurons dedicated to each frequency in the range $1, \dots, \frac{p-1}{2}$. Focusing on a specific frequency ζ, for the sake of simplicity, let us use $\cos_\zeta(x)$ to represent $\cos(2\pi\zeta x/p)$ and $\sin_\zeta(x)$ likewise.

We define

$$a_{[k]} := \sum_{i=1}^{k} a_k$$

and we also define

$$a_{k+1} := -c.$$

For easy of writing, we will write $\cos_\zeta$ as cos and $\sin_\zeta$ as sin. We have the following.

$$\begin{aligned}
& \cos_\zeta(\sum_{i=1}^{k} a_i - c) \\
= & \cos(\sum_{i=1}^{k} a_i - c) \\
= & \cos(a_{[k+1]}) \\
= & \cos(a_{[k]})\cos(a_{k+1}) - \sin(a_{[k]})\sin(a_{k+1}) \\
= & \cos(a_{[k-1]} + a_k)\cos(a_{k+1}) - \sin(a_{[k-1]} + a_k)\sin(a_{k+1}) \\
= & \cos(a_{[k-1]})\cos(a_k)\cos(a_{k+1}) - \sin(a_{[k-1]})\sin(a_k)\cos(a_{k+1}) \\
& - \sin(a_{[k-1]})\cos(a_k)\sin(a_{k+1}) - \cos(a_{[k-1]})\sin(a_k)\sin(a_{k+1}) \\
= & \sum_{b \in \{0,1\}^{k+1}} \prod_{i=1}^{k+1} \cos^{1-b_i}(a_i) \cdot \sin^{b_i}(a_i) \cdot \mathbf{1}[\sum_{i=1}^{k+1} b_i \% 2 = 0] \cdot (-1)^{\mathbf{1}[\sum_{i=1}^{k+1} b_i \% 4 = 2]}, \qquad (25)
\end{aligned}$$

where the first step comes from the simplicity of writing, the second step comes from the definition of $a_{[k+1]}$ and a_{k+1}, the third step comes from the trigonometric function, the fourth step also follows trigonometric function, and the last step comes from the below two observations:

- First, we observe that $\cos(a+b) = \cos(a)\cos(b) - \sin(a)\sin(b)$ and $\sin(a+b) = \sin(a)\cos(b) + \cos(a)\sin(b)$. When we split cos once, we will remove one cos product and we may add zero or two sin products. When we split sin once, we may remove one sin product and we will add one sin product as well. Thus, we can observe that the number of sin products in each term is always even.
- Second, we observe only when we split cos and add two sin products will introduce a -1 is this term. Thus, when the number of sin products $\%4 = 2$, the sign of this term will be -1. Otherwise, it will be $+1$.

Note that we have 2^k non-zero term in Eq. (25). Each of these 2^k terms can be implemented by 2^{k-1} neurons $\phi_1, \cdots, \phi_{2^{k-1}}$.

For the i-th neuron, we have

$$\phi_i = (\sum_{j=1}^{k} u_{i,j}(a_j))^k \cdot w_i(c).$$

By changing $(\theta_{i,j})^*$, we can change the $u_{i,j}(a_j)$ from $\cos_\zeta(\cdot)$ to be $-\cos_\zeta(\cdot)$ or $\sin_\zeta(\cdot)$ or $-\sin_\zeta(\cdot)$. Denote $\theta_{u_i}^*$ as $(\theta_{i,a_i})^*$.

For simplicity, let d_i denote the i-th product in one term of Eq. (25). By fact that

$$2^k \cdot k! \cdot \prod_{i=1}^k d_i = \sum_{c \in \{-1,+1\}^k} (-1)^{(k - \sum_{i=1}^k c_i)/2} (\sum_{j=1}^k c_j d_j)^k,$$

each term can be constructed by 2^{k-1} neurons (note that there is a symmetric effect so we only need half terms). Based on Eq. (25) and the above fact with carefully check, we can see that $\theta^*_{u_1} + \cdots + \theta^*_{u_k} = \theta^*_w$. Thus, we need $2^k \cdot 2^{k-1} \cdot \frac{p-1}{2}$ neurons in total.

When we include such $2^k \cdot 2^{k-1}$ neurons for all frequencies $\zeta \in \{1, \ldots, \frac{p-1}{2}\}$, we have the network will calculate the following function

$$\begin{aligned} f(a_1, \ldots, a_k, c) = & \sum_{\zeta=1}^{(p-1)/2} \cos_\zeta(\sum_{i=1}^k a_i - c) \\ = & \sum_{\zeta=1}^{p-1} \frac{1}{2} \cdot \exp(2\pi \mathbf{i} \zeta (\sum_{i=1}^k a_i - c)/p) \\ = & \begin{cases} \frac{p-1}{2} & \text{if } \sum_{i=1}^k a_i = c \\ 0 & \text{otherwise} \end{cases} \end{aligned}$$

where the first step comes from the definition of $f(a_1, \ldots, a_k, c)$, the second step comes from Euler's formula, the last step comes from the properties of discrete Fourier transform.

The scaling parameter β for each neuron can be adjusted to ensure that the network possesses an $L_{2,k+1}$-norm of 1. For this network, all data points are positioned on the margin, which implies that $q = \mathrm{unif}(\mathbb{Z}_p)$ naturally supports points along the margin, aligning with the requirements for q^* presented in Definition 3.5. Additionally, for every input $(a_1, \ldots, a_k)$, the function f assigns the same outcome to all incorrect labels c', thereby fulfilling Condition 3.8. □

F Check Fourier Frequencies

Section F.1 proves all frequencies are used. Section F.2 proves all frequencies are used for general k version.

F.1 All Frequencies are Used

Let $f : \mathbb{Z}_p^4 \to \mathbb{C}$. Its multi-dimensional discrete Fourier transform is defined as:

$$\begin{aligned} & \widehat{f}(j_1, j_2, j_3, j_4) \\ := & \sum_{a_1 \in \mathbb{Z}_p} e^{-2\pi \mathbf{i} \cdot j_1 a_1 / p} (\sum_{a_2 \in \mathbb{Z}_p} e^{-2\pi \mathbf{i} \cdot j_2 a_2 / p} (\sum_{a_3 \in \mathbb{Z}_p} e^{-2\pi \mathbf{i} \cdot j_3 a_3 / p} (\sum_{c \in \mathbb{Z}_p} e^{-2\pi \mathbf{i} \cdot j_4 c / p} f(a_1, a_2, a_3, c)))). \end{aligned}$$

Lemma F.1. *When $k = 3$, if the following conditions hold*

- *We adopt the uniform class weighting: $\forall c' \neq a_1 + a_2 + a_3, \quad \tau(a_1, a_2, a_3)[c'] := 1/(p-1)$.*
- *f is the maximum $L_{2,4}$-margin solution.*

Then, for any $j_1 = j_2 = j_3 = -j_4 \neq 0$, we have $\widehat{f}(j_1, j_2, j_3, j_4) > 0$.

Proof. In this proof, let $j_1, j_2, j_3, j_4 \in \mathbb{Z}$, and $\theta_u = \theta^*_u \cdot \frac{p}{2\pi}$ to simplify the notation. By Lemma D.4,

$$u_1(a_1) = \sqrt{\frac{1}{2p}} \cos_p(\theta_{u_1} + \zeta a_1). \tag{26}$$

Let

$$\begin{aligned}
& f(a_1,a_2,a_3,c) \\
= & \sum_{h=1}^{H} \phi_h(a_1,a_2,a_3,c) \\
= & \sum_{h=1}^{H} (u_{h,1}(a_1)+u_{h,2}(a_2)+u_{h,3}(a_3))^3 w_h(c) \\
= & (\frac{1}{2p})^2 \sum_{h=1}^{H} (\cos_p(\theta_{u_{h,1}}+\zeta_h a_1)+\cos_p(\theta_{u_{h,2}}+\zeta_h a_2)+\cos_p(\theta_{u_{h,3}}+\zeta_h a_3))^3 \cos_p(\theta_{w_h}+\zeta_h c)
\end{aligned}$$

where each neuron conforms to the previously established form, and the width H function is an arbitrary margin-maximizing network. The first step is from the definition of $f(a_1,a_2,a_3,c)$, the subsequent step on the definition of $\phi_h(a_1,a_2,a_3,c)$, and the final step is justified by Eq. (26).

We can divide each ϕ into ten terms:

$$\begin{aligned}
& \phi(a_1,a_2,a_3,c) \\
= & \phi^{(1)}(a_1,a_2,a_3,c)+\cdots+\phi^{(10)}(a_1,a_2,a_3,c) \\
= & \big(u_1(a_1)^3+u_2(a_2)^3+u_3(a_3)^3+3u_1(a_1)^2u_2(a_2)+3u_1(a_1)^2u_3(a_3)+3u_2(a_2)^2u_1(a_1) \\
& +3u_2(a_2)^2u_3(a_3)+3u_3(a_3)^2u_1(a_1)+3u_3(a_3)^2u_2(a_2)+6u_1(a_1)u_2(a_2)u_3(a_3)\big)w(c).
\end{aligned}$$

Note, $\rho = e^{2\pi \mathbf{i}/p}$. $\widehat{\phi}_1(j_1,j_2,j_3,j_4)$ is nonzero only for $j_1 = 0$, and $\widehat{\phi}_4(j_1,j_2,j_3,j_4)$ is nonzero only for $j_1 = j_2 = 0$. Similar to other terms. For the tenth term, we have

$$\begin{aligned}
\widehat{\phi}_{10}(j_1,j_2,j_3,j_4) = & 6 \sum_{a_1,a_2,a_3,c\in\mathbb{Z}_p} u_1(a_1)u_2(a_2)u_3(a_3)w(c)\rho^{-(j_1a_1+j_2a_2+j_3a_3+j_4c)} \\
= & 6\widehat{u}_1(j_1)\widehat{u}_2(j_2)\widehat{u}_3(j_3)\widehat{w}(j_4).
\end{aligned}$$

In particular,

$$\begin{aligned}
\widehat{u}_1(j_1) = & \sum_{a_1\in\mathbb{Z}_p} \sqrt{\frac{1}{2p}}\cos_p(\theta_{u_1}+\zeta a_1)\rho^{-j_1a_1} \\
= & (8p)^{-1/2} \sum_{a_1\in\mathbb{Z}_p} (\rho^{\theta_{u_1}+\zeta a_1}+\rho^{-(\theta_{u_1}+\zeta a_1)})\rho^{-j_1a_1} \\
= & (8p)^{-1/2}(\rho^{\theta_{u_1}} \sum_{a_1\in\mathbb{Z}_p} \rho^{(\zeta-j_1)a_1}+\rho^{-\theta_{u_1}} \sum_{a_1\in\mathbb{Z}_p} \rho^{-(\zeta+j_1)a_1}) \\
= & \begin{cases} \sqrt{p/8}\cdot\rho^{\theta_{u_1}} & \text{if } j_1 = +\zeta \\ \sqrt{p/8}\cdot\rho^{-\theta_{u_1}} & \text{if } j_1 = -\zeta \\ 0 & \text{otherwise} \end{cases}
\end{aligned}$$

where the first step comes from $\widehat{u}_1(j_1)$ definition, the second step comes from Euler's formula, the third step comes from simple algebra, the last step comes from the properties of discrete Fourier transform. Similarly for $\widehat{u}_2, \widehat{u}_3$ and $\widehat{w}$. As we consider ζ to be nonzero, we ignore the $\zeta = 0$ case. Hence, $\widehat{\phi}_{10}(j_1,j_2,j_3,j_4)$ is nonzero only when j_1,j_2,j_3,j_4 are all $\pm\zeta$. We can summarize that $\widehat{\phi}(j_1,j_2,j_3,j_4)$ can only be nonzero if one of the following satisfies:

- $j_1 \cdot j_2 \cdot j_3 = 0$

- $j_1, j_2, j_3, j_4 = \pm\zeta$.

Setting aside the previously discussed points, it's established in Lemma C.2 that the function f maintains a consistent margin for various inputs as well as over different classes, i.e., f can be broken down as

$$f(a_1, a_2, a_3, c) = f_1(a_1, a_2, a_3, c) + f_2(a_1, a_2, a_3, c)$$

where

$$f_1(a_1, a_2, a_3, c) = F(a_1, a_2, a_3)$$

for some $F : \mathbb{Z}_p \times \mathbb{Z}_p \times \mathbb{Z}_p \to \mathbb{R}$, and

$$f_2(a_1, a_2, a_3, c) = \lambda \cdot \mathbf{1}_{a_1+a_2+a_3=c}$$

where $\lambda > 0$ is the margin of f. Then, we have the DFT of f_1 and f_2 are

$$\widehat{f}_1(j_1, j_2, j_3, j_4) = \begin{cases} \widehat{F}(j_1, j_2, j_3) & \text{if } j_4 = 0 \\ 0 & \text{otherwise} \end{cases}$$

and

$$\widehat{f}_2(j_1, j_2, j_3, j_4) = \begin{cases} \lambda p^3 & \text{if } j_1 = j_2 = j_3 = -j_4 \\ 0 & \text{otherwise} \end{cases}.$$

Hence, when $j_1 = j_2 = j_3 = -j_4 \neq 0$, we must have $\widehat{f}(j_1, j_2, j_3, j_4) > 0$. □

F.2 All Frequencies are Used for General k Version

Let $f : \mathbb{Z}_p^{k+1} \to \mathbb{C}$. Its multi-dimensional discrete Fourier transform is defined as:

$$\begin{aligned} & \widehat{f}(j_1, \ldots, j_{k+1}) \\ := & \sum_{a_1 \in \mathbb{Z}_p} e^{-2\pi \mathbf{i} \cdot j_1 a_1 / p} (\ldots (\sum_{a_k \in \mathbb{Z}_p} e^{-2\pi \mathbf{i} \cdot j_k a_k / p} (\sum_{c \in \mathbb{Z}_p} e^{-2\pi \mathbf{i} \cdot j_{k+1} c / p} f(a_1, \ldots, a_k, c))). \end{aligned}$$

Lemma F.2. *If the following conditions hold*

- *We adopt the uniform class weighting:* $\forall c' \neq a_1 + \cdots + a_k, \quad \tau(a_1, \ldots, a_k)[c'] := 1/(p-1)$.
- f *is the maximum* $L_{2,k+1}$*-margin solution.*

Then, for any $j_1 = \cdots = j_k = -j_{k+1} \neq 0$*, we have* $\widehat{f}(j_1, \ldots, j_{k+1}) > 0$.

Proof. For this proof, for all $j_1, \ldots, j_{k+1} \in \mathbb{Z}$, to simplify the notation, let $\theta_u = \theta_u^* \cdot \frac{p}{2\pi}$, by Lemma D.8, so

$$u_1(a_1) = \sqrt{\frac{2}{(k+1)p}} \cos_p(\theta_{u_1} + \zeta a_1). \tag{27}$$

Let

$$
\begin{aligned}
f(a_1,\ldots,a_k,c) &= \sum_{h=1}^{H} \phi_h(a_1,\ldots,a_k,c) \\
&= \sum_{h=1}^{H} (u_{h,1}(a_1)+\cdots+u_{h,k}(a_k))^k w_h(c) \\
&= (\frac{2}{(k+1)p})^{(k+1)/2} \sum_{h=1}^{H} (\cos_p(\theta_{u_{h,1}}+\zeta_h a_1)+\cdots+\cos_p(\theta_{u_{h,k}}+\zeta_h a_k))^k \cos_p(\theta_{w_h}+\zeta_h c)
\end{aligned}
$$

where each neuron conforms to the previously established form, and the width H function is an arbitrary margin-maximizing network. The first step is based on the definition of $f(a_1,\ldots,a_k,c)$, the subsequent step on the definition of $\phi_h(a_1,\ldots,a_k,c)$, and the final step is justified by Eq. (27).

Each neuron ϕ we have

$$
\begin{aligned}
\widehat{\phi}(j_1,\ldots,j_k,j_{k+1}) &= k! \sum_{a_1,\ldots,a_k,c\in\mathbb{Z}_p} w(c)\rho^{-(j_1a_1+\cdots+j_ka_k+j_{k+1}c)} \prod_{i=1}^{k} u_i(a_i) \\
&= k!\widehat{w}(j_{k+1}) \prod_{i=1}^{k} \widehat{u}_i(j_i).
\end{aligned}
$$

In particular,

$$
\begin{aligned}
\widehat{u}_1(j_1) &= \sum_{a_1\in\mathbb{Z}_p} \sqrt{\frac{2}{(k+1)p}} \cos_p(\theta_{u_1}+\zeta a_1)\rho^{-j_1a_1} \\
&= \sqrt{\frac{1}{2(k+1)p}} \sum_{a_1\in\mathbb{Z}_p} (\rho^{\theta_{u_1}+\zeta a_1}+\rho^{-(\theta_{u_1}+\zeta a_1)})\rho^{-j_1a_1} \\
&= \sqrt{\frac{1}{2(k+1)p}} (\rho^{\theta_{u_1}} \sum_{a_1\in\mathbb{Z}_p} \rho^{(\zeta-j_1)a_1} + \rho^{-\theta_{u_1}} \sum_{a_1\in\mathbb{Z}_p} \rho^{-(\zeta+j_1)a_1}) \\
&= \begin{cases} \sqrt{\frac{p}{2(k+1)}} \cdot \rho^{\theta_{u_1}} & \text{if } j_1 = +\zeta \\ \sqrt{\frac{p}{2(k+1)}} \cdot \rho^{-\theta_{u_1}} & \text{if } j_1 = -\zeta \\ 0 & \text{otherwise,} \end{cases}
\end{aligned}
$$

where the first step comes from $\widehat{u}_1(j_1)$ definition, the second step comes from Euler's formula, the third step comes from simple algebra, the last step comes from the properties of discrete Fourier transform. Similarly for $\widehat{u}_i$ and $\widehat{w}$. We consider ζ to be nonzero, so we ignore the $\zeta = 0$ case. Hence, $\widehat{\phi}(j_1,\ldots,j_k,j_{k+1})$ is nonzero only when $j_1,\ldots,j_k,j_{k+1}$ are all $\pm\zeta$. We can summarize that $\widehat{\phi}(j_1,\ldots,j_k,j_{k+1})$ can only be nonzero if one of the below conditions satisfies:

- $\prod_{i=1}^{k} j_i = 0$
- $j_1,\ldots,j_k,j_{k+1} = \pm\zeta$.

Setting aside the previously discussed points, it's established in Lemma C.2 that the function f maintains a consistent margin for various inputs as well as over different classes, i.e., f can be broken down as

$$
f(a_1,\ldots,a_k,c) = f_1(a_1,\ldots,a_k,c) + f_2(a_1,\ldots,a_k,c)
$$

where

$$f_1(a_1, \dots, a_k, c) = F(a_1, \dots, a_k)$$

for some $F : \mathbb{Z}_p^k \to \mathbb{R}$, and

$$f_2(a_1, \dots, a_k, c) = \lambda \cdot \mathbf{1}_{a_1 + \cdots + a_k = c}$$

where $\lambda > 0$ is the margin of f. Then, we have the DFT of f_1 and f_2 are

$$\widehat{f}_1(j_1, \dots, j_k, j_{k+1}) = \begin{cases} \widehat{F}(j_1, \dots, j_k) & \text{if } j_{k+1} = 0 \\ 0 & \text{otherwise} \end{cases}$$

and

$$\widehat{f}_2(j_1, \dots, j_k, j_{k+1}) = \begin{cases} \lambda p^k & \text{if } j_1 = \cdots = j_k = -j_{k+1} \\ 0 & \text{otherwise} \end{cases}.$$

Hence, when $j_1 = \cdots = j_k = -j_{k+1} \neq 0$, we must have $\widehat{f}(j_1, \dots, j_k, j_{k+1}) > 0$. □

G Proof of Main Result

Section G.1 proves the main result for $k = 3$. Section G.2 proves the general k version of our main result.

G.1 Main result for $k = 3$

Theorem G.1. *When $k = 3$, let $f(\theta, x)$ be the one-hidden layer networks defined in Section 3. If the following conditions hold*

- *We adopt the uniform class weighting: $\forall c' \neq a_1 + a_2 + a_3, \quad \tau(a_1, a_2, a_3)[c'] := 1/(p-1)$.*
- *$m \geq 16(p-1)$ neurons.*

Then we have the maximum $L_{2,4}$-margin network satisfying:

- *The maximum $L_{2,4}$-margin for a given dataset D_p is:*

$$\gamma^* = \frac{3}{16} \cdot \frac{1}{p(p-1)}.$$

- *For each neuron $\phi(\{u_1, u_2, u_3, w\}; a_1, a_2, a_3)$, there is a constant scalar $\beta \in \mathbb{R}$ and a frequency $\zeta \in \{1, \dots, \frac{p-1}{2}\}$ satisfying*

$$\begin{aligned} u_1(a_1) &= \beta \cdot \cos(\theta_{u_1}^* + 2\pi\zeta a_1/p) \\ u_2(a_2) &= \beta \cdot \cos(\theta_{u_2}^* + 2\pi\zeta a_2/p) \\ u_3(a_3) &= \beta \cdot \cos(\theta_{u_3}^* + 2\pi\zeta a_3/p) \\ w(c) &= \beta \cdot \cos(\theta_w^* + 2\pi\zeta c/p) \end{aligned}$$

  where $\theta_{u_1}^*, \theta_{u_2}^*, \theta_{u_3}^*, \theta_w^* \in \mathbb{R}$ are some phase offsets satisfying $\theta_{u_1}^* + \theta_{u_2}^* + \theta_{u_3}^* = \theta_w^*$.

- *For each frequency $\zeta \in \{1, \dots, \frac{p-1}{2}\}$, there exists one neuron using this frequency only.*

Proof. By Lemma D.4, we get the single neuron class-weighted margin solution set $\Omega_q^{'*}$ satisfying Condition 3.8 and γ^*.

By Lemma E.2 and Lemma C.1, we can construct network θ^* which uses neurons in $\Omega_q^{'*}$ and satisfies Condition 3.8 and Definition 3.5 with respect to $q = \mathrm{unif}(\mathbb{Z}_p)$. By Lemma C.2, we know it is the maximum-margin solution.

By Lemma F.1, when $j_1 = j_2 = j_3 = -j_4 \neq 0$, we must have $\widehat{f}(j_1, j_2, j_3, j_4) > 0$. However, as discrete Fourier transform $\widehat{\phi}$ of each neuron is nonzero, for each frequency, we must have that there exists one neuron using it.

□

G.2 Main Result for General k Version

Theorem G.2 (Formal version of Theorem 4.1)**.** *Let $f(\theta, x)$ be the one-hidden layer networks defined in Section 3. If the following conditions hold*

- *We adopt the uniform class weighting: $\forall c' \neq a_1 + \cdots + a_k, \quad \tau(a_1, \dots, a_k)[c'] := 1/(p-1)$.*
- *$m \geq 2^{2k-1} \cdot \frac{p-1}{2}$ neurons.*

Then we have the maximum $L_{2,k+1}$-margin network satisfying:

- *The maximum $L_{2,k+1}$-margin for a given dataset D_p is:*

$$\gamma^* = \frac{2(k!)}{(2k+2)^{(k+1)/2}(p-1)p^{(k-1)/2}}.$$

- *For each neuron $\phi(\{u_1, \dots, u_k, w\}; a_1, \dots, a_k)$ there is a constant scalar $\beta \in \mathbb{R}$ and a frequency $\zeta \in \{1, \dots, \frac{p-1}{2}\}$ satisfying*

$$\begin{aligned} u_1(a_1) &= \beta \cdot \cos(\theta_{u_1}^* + 2\pi\zeta a_1/p) \\ &\cdots \\ u_k(a_k) &= \beta \cdot \cos(\theta_{u_k}^* + 2\pi\zeta a_k/p) \\ w(c) &= \beta \cdot \cos(\theta_w^* + 2\pi\zeta c/p) \end{aligned}$$

  where $\theta_{u_1}^*, \dots, \theta_{u_k}^*, \theta_w^* \in \mathbb{R}$ are some phase offsets satisfying $\theta_{u_1}^* + \cdots + \theta_{u_k}^* = \theta_w^*$.

- *For every frequency $\zeta \in \{1, \dots, \frac{p-1}{2}\}$, there exists one neuron using this frequency only.*

Proof. Follow the same proof sketch as Theorem G.1 by Lemma D.8, Condition 3.8, Lemma E.3, Lemma C.1, Definition 3.5, Lemma C.2, Lemma F.2.

□

H More Empirical Details and Results

H.1 Implement Details

Licenses for Existing Assets & Open Access to Data and Code. Our code is based on a brilliant open source repository, `https://github.com/Sea-Snell/grokking`, which requires MIT License. We provide all of our codes in the supplemental material, including dataset generation code. We do not require open data access as we run experiments on synthetic datasets, i.e., modular addition.

Experimental Result Reproducibility. We provide all of our codes in the supplemental material with a clear README file and clear configuration files for our experiments reproducibility.

Experimental Setting/Details & Experiment Statistical Significance. The detailed configuration can be found in supplemental material. We make a copy version here for convenience.

For two-layer neural network training, we have the following details:

- number of data loader workers: 4
- batch size: 1024
- learning rate: 5×10^{-3}
- regularization strength λ: 0.005
- AdamW hyper-parameter (β_1, β_2): $(0.9, 0.98)$
- warm-up steps: 10

For one-layer Transformer training, we have the following details:

- number of data loader workers: 4
- batch size: 1024
- learning rate: 1×10^{-3}
- regularization strength λ: 0.001
- AdamW hyper-parameter (β_1, β_2): $(0.9, 0.98)$
- warm-up steps: 10

All results we ran 3 times with different random seeds. In Figure 4, we reported the mean and variance range.

Experiments Compute Resources. All experiments is conducted on single A100 40G NVIDIA GPU. All experiments can be finished in at most three days.

H.2 One-hidden Layer Neural Network

In Figure 5 and Figure 6, we use SGD to train a two-layer network with $m = 1536 = 2^{2k-2} \cdot (p-1)$ neurons, i.e., Eq. (2), on $k = 3$-sum mod-$p = 97$ addition dataset, i.e., Eq. (1). In Figure 7 and Figure 8, we use SGD to train a two-layer network with $m = 5632 = 2^{2k-2} \cdot (p-1)$ neurons, i.e., Eq. (2), on $k = 5$-sum mod-$p = 23$ addition dataset, i.e., Eq. (1).

Figure 5 and Figure 7 show that the networks trained with stochastic gradient descent have single-frequency hidden neurons, which support our analysis in Lemma 4.2. Furthermore, Figure 6 and Figure 8 demonstrate that the network will learn all frequencies in the Fourier spectrum which is consistent with our analysis in Lemma 4.3. Together, they verify our main results in Theorem 4.1 and show that the network trained by SGD prefers to learn Fourier-based circuits.

H.3 One-layer Transformer

In Figure 9 , we train a one-layer transformer with $m = 160$ heads attention, on $k = 3$-sum mod-$p = 61$ addition dataset, i.e., Eq. (1). In Figure 10 , we train a one-layer transformer with $m = 160$ heads attention, on $k = 5$-sum mod-$p = 17$ addition dataset, i.e., Eq. (1).

Figure 9 and Figure 10 show that the one-layer transformer trained with stochastic gradient descent learns 2-dim cosine shape attention matrices, which is similar to one-hidden layer neural networks in Figure 5 and Figure 7. This means that the attention layer has a similar learning mechanism to neural networks in the modular arithmetic task, where it prefers to learn Fourier-based circuits when trained by SGD.

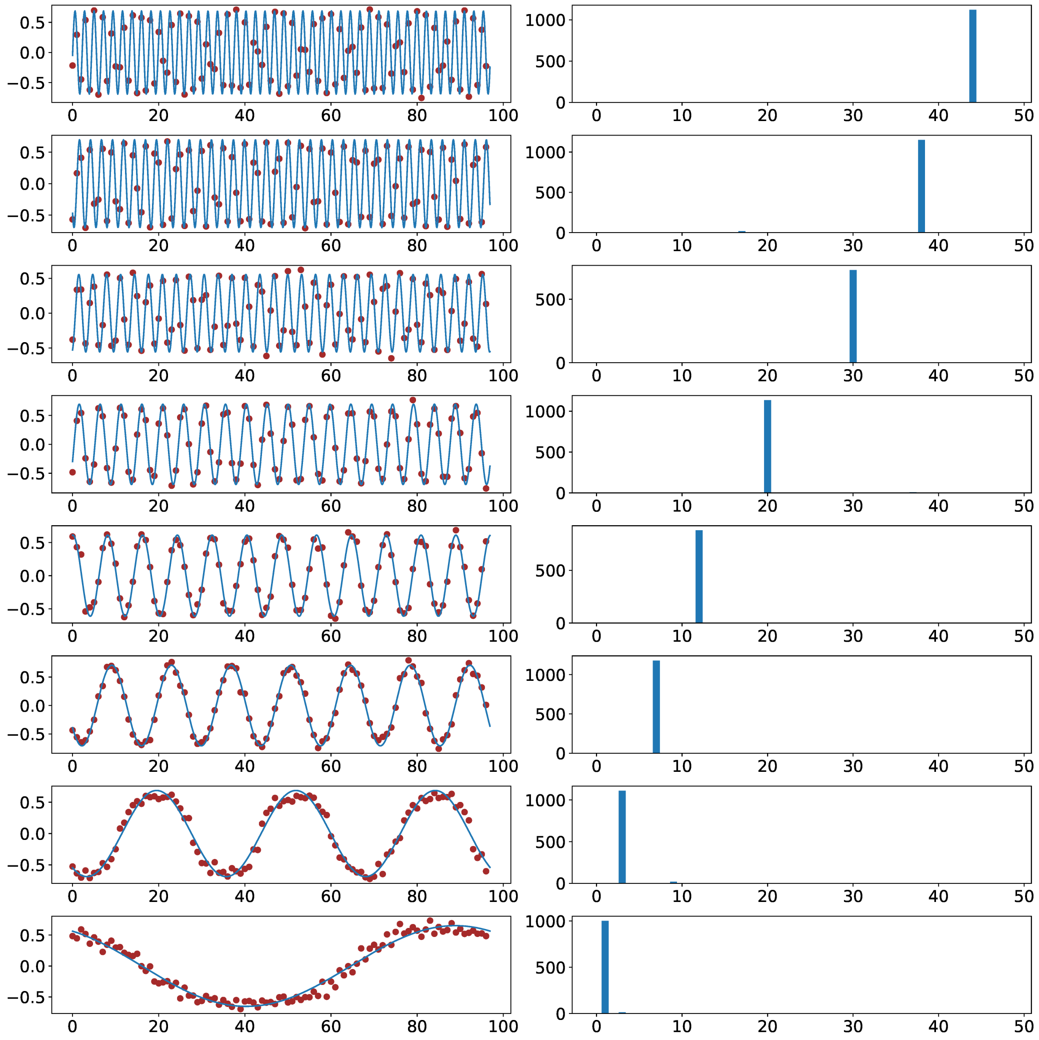

Figure 5: Cosine shape of the trained embeddings (hidden layer weights) and corresponding power of Fourier spectrum. The two-layer network with $m = 1536$ neurons is trained on $k = 3$-sum mod-$p = 97$ addition dataset. We even split the whole datasets ($p^k = 97^3$ data points) into the training and test datasets. Every row represents a random neuron from the network. The left figure shows the final trained embeddings, with red dots indicating the true weight values, and the pale blue interpolation is achieved by identifying the function that shares the same Fourier spectrum. The right figure shows their Fourier power spectrum. The results in these figures are consistent with our analysis statements in Lemma 4.2.

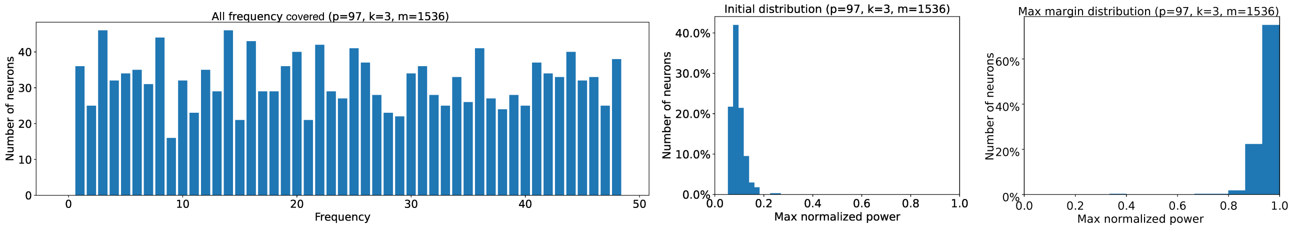

Figure 6: All Fourier spectrum frequencies being covered and the maximum normalized power of the embeddings (hidden layer weights). The one-hidden layer network with $m = 1536$ neurons is trained on $k = 3$-sum mod-$p = 97$ addition dataset. We denote $\widehat{u}[i]$ as the Fourier transform of $u[i]$. Let $\max_i |\widehat{u}[i]|^2/(\sum |\widehat{u}[j]|^2)$ be the maximum normalized power. Mapping each neuron to its maximum normalized power frequency, (a) shows the final frequency distribution of the embeddings. Similar to our construction analysis in Lemma 4.3, we have an almost uniform distribution over all frequencies. (b) shows the maximum normalized power of the neural network with random initialization. (c) shows, in frequency space, the embeddings of the final trained network are one-sparse, i.e., maximum normalized power being almost 1 for all neurons. This is consistent with our maximum-margin analysis results in Lemma 4.3.

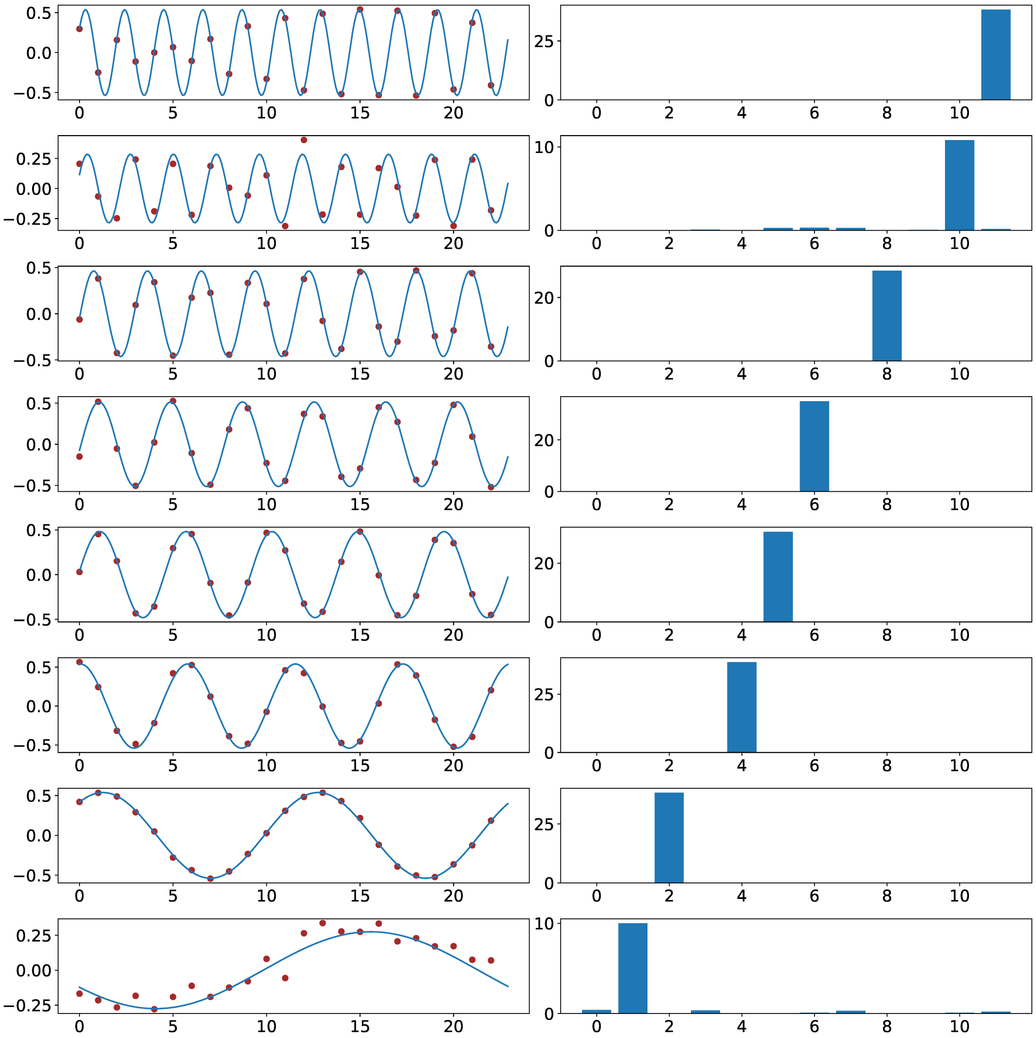

Figure 7: Cosine shape of the trained embeddings (hidden layer weights) and corresponding power of Fourier spectrum. The two-layer network with $m = 5632$ neurons is trained on $k = 5$-sum mod-$p = 23$ addition dataset. We even split the whole datasets ($p^k = 23^5$ data points) into the training and test datasets. Every row represents a random neuron from the network. The left figure shows the final trained embeddings, with red dots indicating the true weight values, and the pale blue interpolation is achieved by identifying the function that shares the same Fourier spectrum. The right figure shows their Fourier power spectrum. The results in these figures are consistent with our analysis statements in Lemma 4.2.

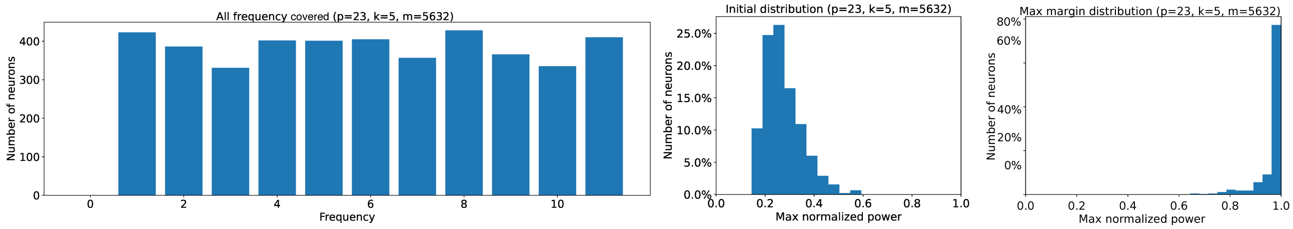

Figure 8: All Fourier spectrum frequencies being covered and the maximum normalized power of the embeddings (hidden layer weights). The one-hidden layer network with $m = 5632$ neurons is trained on $k = 5$-sum mod-$p = 23$ addition dataset. We denote $\widehat{u}[i]$ as the Fourier transform of $u[i]$. Let $\max_i |\widehat{u}[i]|^2 / (\sum |\widehat{u}[j]|^2)$ be the maximum normalized power. Mapping each neuron to its maximum normalized power frequency, (a) shows the final frequency distribution of the embeddings. Similar to our construction analysis in Lemma 4.3, we have an almost uniform distribution over all frequencies. (b) shows the maximum normalized power of the neural network with random initialization. (c) shows, in frequency space, the embeddings of the final trained network are one-sparse, i.e., maximum normalized power being almost 1 for all neurons. This is consistent with our maximum-margin analysis results in Lemma 4.3.

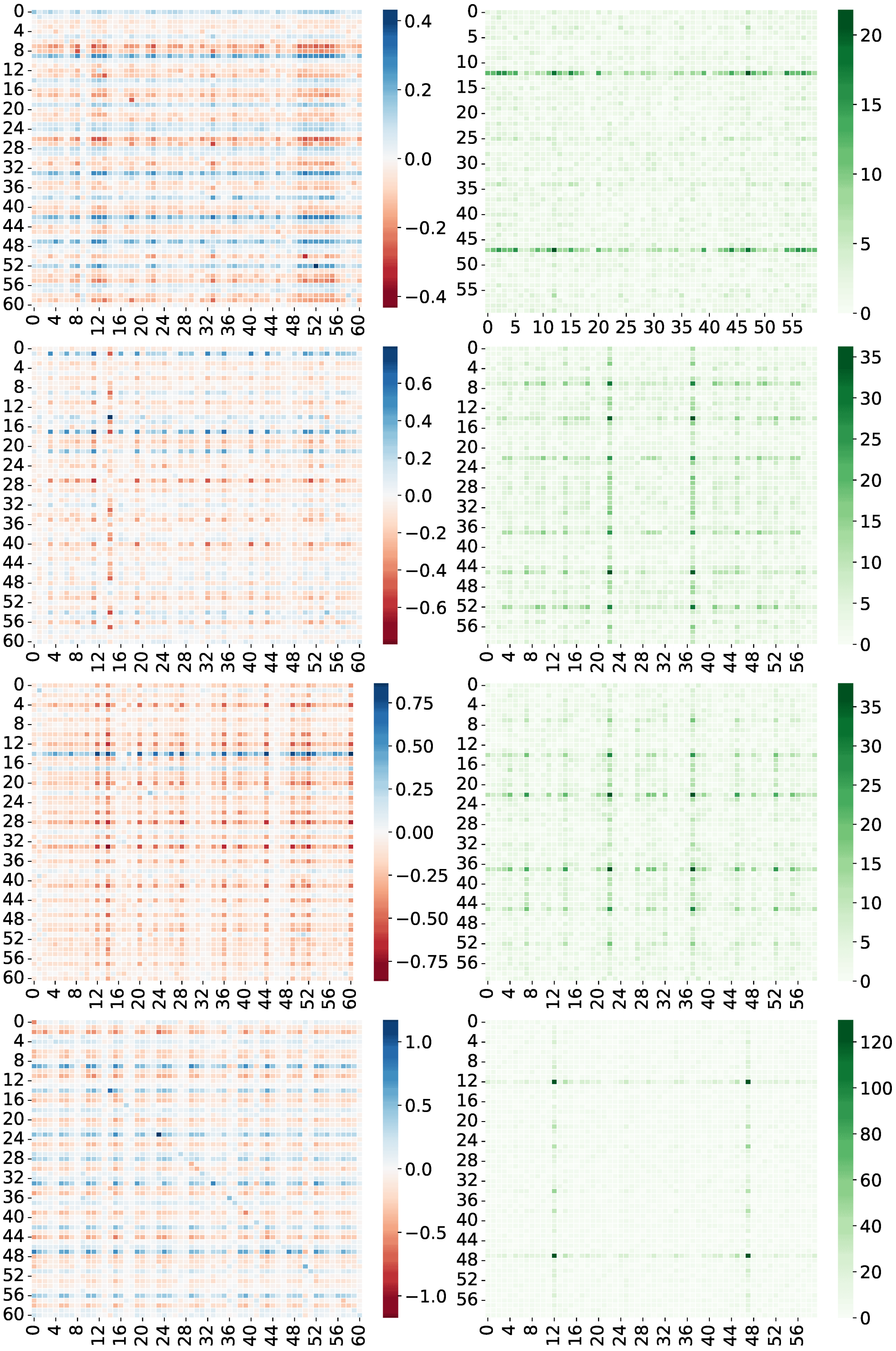

Figure 9: 2-dimension cosine shape of the trained W^{KQ} (attention weights) and their Fourier power spectrum. The one-layer transformer with attention heads $m = 160$ is trained on $k = 3$-sum mod-$p = 61$ addition dataset. We even split the whole datasets ($p^k = 61^3$ data points) into training and test datasets. Every row represents a random attention head from the transformer. The left figure shows the final trained attention weights being an apparent 2-dim cosine shape. The right figure shows their 2-dim Fourier power spectrum. The results in these figures are consistent with Figure 5.

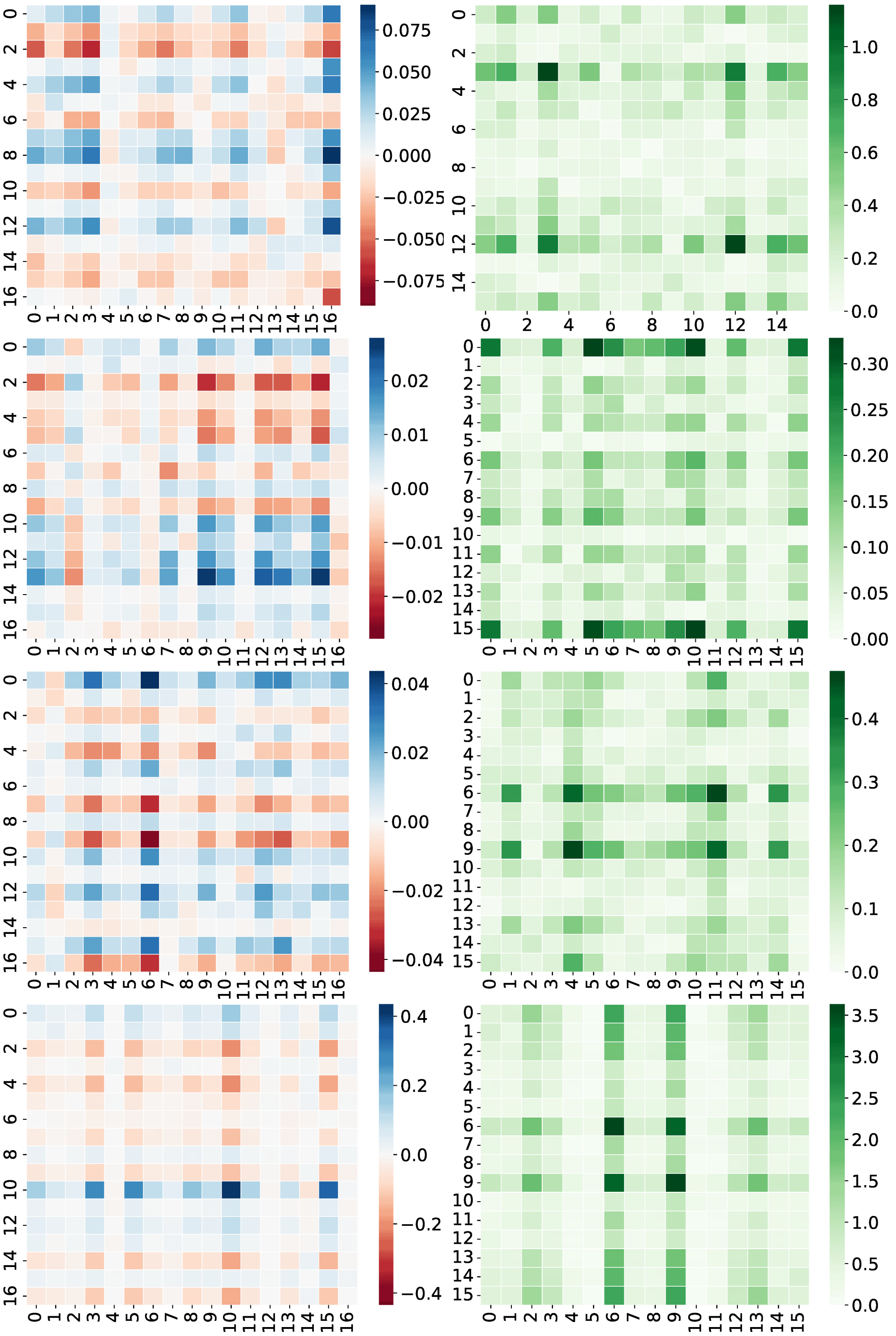

Figure 10: 2-dimension cosine shape of the trained W^{KQ} (attention weights) and their Fourier power spectrum. The one-layer transformer with attention heads $m = 160$ is trained on $k = 5$-sum mod-$p = 17$ addition dataset. We even split the whole datasets ($p^k = 17^5$ data points) into training and test datasets. Every row represents a random attention head from the transformer. The left figure shows the final trained attention weights being an apparent 2-dim cosine shape. The right figure shows their 2-dim Fourier power spectrum. The results in these figures are consistent with Figure 7.